Chapter 1 Introduction

Numerical micrmagnetic analysis has been widely applied in mag -netic recording and spintornics field, including static and dynamic state concern. Currently, the storage capability and density are getting remarkable advances. From conventional model, SAF, perpendicular, pattern media to HARM, the demand for high density and small dimension recording increases dramatically. Macroscopic experiment result can't demonstrate the microscope behavior in detail now and future.

Some novel media models have been tracking more and more attractions recently, including ECC media, exchange spring, and graded media. People intend to overcome the current magnetic recording limit by these media design. Varieties of different models are developed to explain the switching mechanism of these systems. For example, the domain wall assisted switching and the related micro-mechanism. Nowadays the advanced mathematical and computational architecture really much benefit this art of micromagnetic simulation, giving a great help of these study.

Different numerical methods for approaching the microscopy magnetic behavior are also being discussed by different groups. Multi-scale method (atomic scale approach) has been shown more precise for large spatial exchange variation interface, comparing with normal

micromagnetic method.

It's obvious that micromagnetic simulation is playing a prosperous role in media. The database created by simulation work provides a helpful guideline of film structure design, both geometric and physical parameters selected. Suess's work is the hot topic, graded media, is a good example. By this concern, National Institute of Standard and Technology(NIST) publics four standard problems on its website, to test other new micromagnetic programming and numerical approaches. Many hart topics can be seen from the point of micromagnetic. For example, in ECC/exchange spring media, the domain wall propagation mechanism and moment critical switching angle. Many simulation works dedicate in this field, energy landscape [1], and thermal reversal behavior [2].

Moreover, as far as the read/write speed enhancing, dynamic effect should not be neglected any more. As a result, the design of modern ultra-fast magnetic recording devices can not be done out of the framework of magnetization dynamic. This phenomenon is widely discussed by in-situ MFM image, indicating different z-component of magnetization. Micromagntic simulation calculates the most stable magnetization state in the lowest energy potential, by Euler or minimum and other numerical method.

The exchange coupled composite of multi-layer structure has been investigated for some time in our group. In our design, the CoCrPt-SiO_2/Pt assisting layer plays an important role. CoCrPt is the one

of the most promising candidates for perpendicular recording because that it has been wide-spreading studied in longitudinal media. Its properties are also further improved recently. Oxide granular CoCrPt-SiO_2 is proposed to induce better grain isolation via rich oxygen boundaries, with no epitaxial CoCrPt growth disturbing. This isolated grain can reduce the inter-grain exchange coupling and leads to a higher single-to-noise ratio (SNR). The CoCrPt magnetic properties tendency corresponding to varying exchange coupling and different soft layer number will be studied in this article.

Chapter 2 Background

In order to solve magnetization dynamics, the Landau–Liifshitz–Gilbert (LLG) equation is generally used for the purpose. It's called the semi-discretization approach. The common procedure is as following.

First, we use finite element method(FEM) or finite different method(FDM) to discretize the LLG equation in the special space. The corresponding ordinary differential equations (ODE) and micromagntic Gibbs free energy can be divided into discretiaed version. Second, use a suitable time-stepping method to numerically integrate the ODE systems. Many numerical techniques are available. Here we can use Runke-Kutta method to save the computational time consumption. Finally, apply the Dynamic equation combines with LLG equation. This will be discussed in detail in section 2.2.2.2.

2.1 Finite difference method

The basic principle and finite difference method (FDM) is as following. For a specific continuous physical region, fill it with finite many regular shaped cells. Taking these mesh points into control function, as well as initial and boundary conditions. Then the relations between mesh points and nearby points can be obtained.

2.1.1 Forward, backward and central differences

The fundamental Forward difference is like the following expression of the form,

$$\Delta[f](x) = f(x + h) - f(x)$$

Based of the forward and backward difference, the central difference is given by

$$\delta[f](x) = f(x + 1/2\ h) - f(x - 1/2h)\ ,$$

2.1.2 Finite differences calculation

We just take forward difference as a difference operator, mapping function f to Δf. Taylor's theory can be expressed like this,

$$\Delta = hD + \frac{1}{2!}h^2D^2 + \frac{1}{3!}h^3D^3 + \ldots = e^{hD} - 1$$

Considering value h very approaching to zero, we can define the derivative of a function f at x as following,

$$f'(x) \sim \frac{\Delta[f](x) - \frac{1}{2}\Delta^2[f](x)}{h}$$

$$= -\frac{f(x + 2h) - 4f(x + h) + 3f(x)}{2h}$$

2.1.3 Derivatives with high order

It is well-known that the finite difference approximations to high

order derivatives and differential operators can be obtained in analogous way. An easy example is the central difference approximation of the second derivative of f,

$$f''(x) \sim \frac{\delta^2[f](x)}{h^2} = \frac{f(x+h) - 2f(x) + f(x-h)}{h^2}$$

2.1.4 Finite method

We can notice that, as h goes to zero, the finite difference approaches the differential quotient. So the finite differences can be used to approximate derivatives. The method is much common in dealing with numerical ordinary differential equations and partial differential equations.

2.1.5 Finite different operator

The standard definition of the high order finite difference in mathematical analysis is as following,

$$\Delta_h^n(f, x) := \sum_{k=0}^{n} (-1)^{n-k} \binom{n}{k} f(x + kh)$$

A. Relation with derivatives

In the case of a very smooth function f(x),

$$\lim_{h \to 0} \frac{\Delta_h^n(f, x)}{h^n} = f^{(n)}(x) = D^n(f)$$

Note that D^n is also an operator which can be referred to the differential operator. And there exits a point θ in [x , x + nh] such that,

$$f^{(n)}(\theta) = \frac{\Delta_h^n(f,x)}{h^n}$$

B. Properties

Leibniz rule,

$$\Delta_h^n(f,x) = \int_0^h du_1 \int_0^h du_2 \dots \int_0^h f^{(n)}(x + u_1 + u_2 + \dots + u_n) du_n$$

C. Generalizations

A generalized finite difference operator is commonly defined like,

$$\Delta_h^n(f,x) := \sum_{k=0}^{N} c_k f(x + kh)$$

Generally speaking, this notation of finite different is used in definition of modulus of continuity. And the theory of functional difference equations is also a useful application.

2.2 The finite element micromagnetic model and dynamic equation

The brief overview concept of micromagnetic [3, 4] is introduced here. It's important to take static and dynamic equilibriums into

consideration. The various kinds of interactions involving within ferromagnetic domain at different spatial will be discussed. The second part, Landau–Lifshitz–Gilbert equation (LLG) [5], will be introduced. This equation can explain the spin magnetic momentum of electrons and the widely known relationship with angular momentum though the gyromanetic ratio.

The components supplied with the OOMMF Framework all assume a continuum model of magnetization, within each mixed discretization cell [6-9]. Each cell has one vector (technically, one unit vector and one magnitude) to represent the magnetization over the volume of space that cell represents. This means, it is as samples from a spatially varying volume of magnetization, and not as a collection of discrete moments. The common refinement of the cells at corner is order to deal with the large demagnetization fields, as fig. 2.2.1 [10]. The stable state can be obtained by energy minimizing method or LLG dynamics.

The stray field energy result from the surface charges due to homogeneous magnetization inside each cell like fig. 2.2.2[10], and the exchange energy comes from the nearby cell easy-axis change.

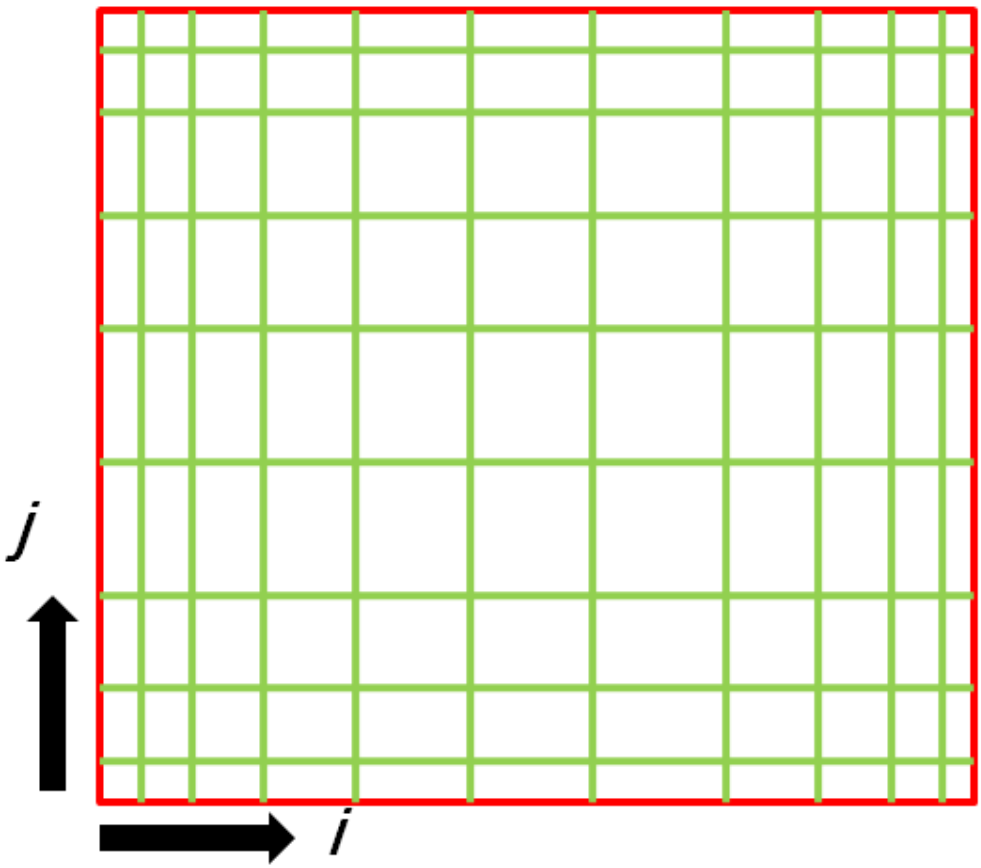

Figure 2.2.1 The refined meshing near edges and corners [10].

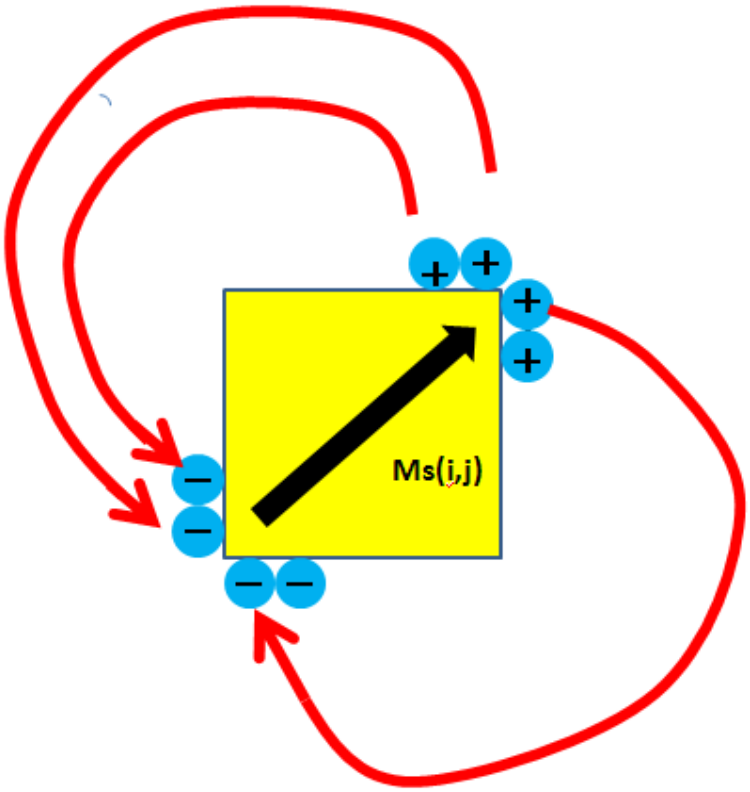

Figure 2.2.2 The surface charges induced stray field [10]

2.2.1 Free energy concern in micromagnetics

Trace back to 1940s, W, F. Brown proposed the first paper on the theory of micromagnetic theory application [11, 12]. This theory filled up the gap the spin structure description based on quantum theory and electromagnetism based on Maxwell's theory. It is considered as the pioneering published paper in this field.

Other conventional micromagnetism theory have been proposed by many books and review papers [13][14][15][16][17]. Here the magnetic free energy can be divided into magnetocrystalline anisotropy, exchange, magnetostatic, and Zeeman energy.

2.2.1.1 Continuum hypothesis

We denote a domain Ω, occupied by a magnetic body. And position vector r belongs to Ω, as well as small regions dV_j inside body. An important assumption here is that, dV_j is large enough to contain big number N of moment μ_j, but small enough that the moment varies smoothly.

It can be described like this,

$$M = \sum_{j}^{N} \mu_j \Big/ dV_j$$

Where M = M(r, t).

2.2.1.2 Anisotropy energy

The basic concept is some special preferring directions of magnetization. Because of the particular symmetries and lattice structure, the anisotropy effect is common in ferromagnetic bodies.

The general form of anisotropy is like,

$$Fan(m) = \int_{\Omega} fan(m)dV$$

A. Uniaxial anisotropy

$$f_{an}(m) = K_0 + K_1 \sin^2\theta + K_2 \sin^4\theta + K_3 \sin^6\theta + \cdots$$

B. Cubic anisotropy

$$f_{an}(m) = K_0 + K_1\left(m_x^2 m_y^2 + m_y^2 m_z^2 + m_z^2 m_x^2\right) + K_2 m_x^2 m_y^2 m_z^2 + \cdots$$

Where the K_i and m_i are the anisotropy and magnetization component, respectively.

2.2.1.3 Exchange energy and interaction

The exchange energy is strongly related to spin-spin interactions, which should be analyzed by view of quantum theory. This kind of interaction can also explain the formation of domains existence [18]. Because it tends to align neighbor spins, forming a uniformly magnetized region.

The energy form can be described as following,

$$W = -2J\sum S_i \bullet S_j$$

$$W = -2jS^2\sum \cos\theta_{i,j} \sim -2JS^2\sum\left(1-\frac{1}{2}\theta_{I,J}^{\ 2}\right) = \text{const.} + JS^2\sum\theta_{i,j}^2 \sim \text{const.} + JS^2\sum(m_i - m_j)^2$$

Here the S_i represents the spin angular momenta, and the $\theta_{i,j}$ is the

angle between vector i and vector j. J is called the nearest neighbor exchange integral.

To replace the microscopic Heisenberg Hamiltonian, the mesoscopic exchange energy [19] term can be presented by the following form,

$$F_{ex} = A\left[(\nabla m_x)^2 + (\nabla m_y)^2 + (\nabla m_z)^2\right]$$

Where exchange constant $A = {}^{1}/_{6}\, n\, JS^2 \sum \Delta_j^2$,

$$F_{ex} = \int_{\Omega} A\left[(\Delta m_x)^2 + (\Delta m_y)^2 + (\Delta m_z)^2\right] dV$$

2.2.1.4 Magnetostatic energy

Considering the first-order variation of the free energy functional,

$$\delta Fm = \int_{\Omega} \frac{1}{2}\mu_0 M H_m dV$$

We can get as following,

$$\delta Fm = \int_{\Omega} \tfrac{1}{2}\mu_0 M_s \delta m \bullet H_m dV - \int_{\Omega} \tfrac{1}{2}\mu_0 M_s m \bullet \delta H_m dV$$

According to reciprocity theorem [20, 21], the above two integrations are the same. So the equation can be rewritten as,

$$\delta Fm = \int_{\Omega} \mu_0 M_s \delta m \bullet H_m dV$$

2.2.1.5 External field induced Zeeman energy

We can observe the potential energy of a continuous magnetic moments distribution, under a external applied field,

$$G_a = \int_{\Omega} \mu_0 M \bullet H_a$$

2.2.1.6 Free energy expression

Summarizing thee above energy concerns, the ferromagnetic body can be written as this form,

$$\begin{aligned} G(M, H_a) &= F_{ex} + F_{an} + F_{am} + G_a \\ &= \int_{\Omega} \{A[(\Delta m_x)^2 + (\Delta m_y)^2 + (\Delta m_z)^2] + \\ &\quad f_{an} + \left(-\frac{1}{2}\right) \mu_0 M \bullet H_m - \mu_0 M \bullet H_a\} dV, \end{aligned}$$

In those energy terms, the long-range magnetostatic energy involves the six-fold integration of the magnetostatic energy. So the complicated computation really depends on a highly computing ability.

2.2.2 The dynamic equation

For current recording device, the remarkable increasing in storage

density and recording speed really brings people more and more attraction on studying in dynamic equation. This is what the Landau – Lifshitz – Gilbert equation (LLG equation) described. There is a brief discussion in this section.

2.2.2.1 Gyromagnetic precession

The precession of spin magnetic moment, around the field,

$$\frac{d\mu_j}{dt} = -\gamma\mu_j \times H$$

Magnetization precession moment,

$$\frac{dM}{dt} = -\gamma M \times H$$

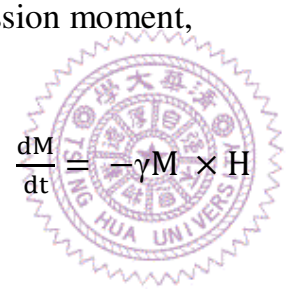

2.2.2.2 The Landau – Lifshitz – Gilbert equation

The damping term and precession energy are competing, described in this LLG equation. Many numerical methods for integrating LLG are proposed, such as midpoint technique [22], and preconditioned finite element method [23]. The following equation is LLG equation.

$$\frac{dM}{dt} = -\gamma M \times H_{eff} + \frac{\alpha}{M_s} \times \frac{dM}{dt}$$

Then consider $a \times (b \times c) = b(a \cdot c) - c(a \cdot b)$ and $M \cdot \frac{dM}{DT} = 0$

The LLG equation can be rearranged as

$$\frac{dM}{dt} = -\gamma M \times H_{eff} - \frac{\gamma\alpha}{M_s} M \times (M \times H_{eff}) - \alpha^2 \frac{dM}{dt}$$

2.3 Micromagnetic simulation – development and current state

Advanced computational micromagnetism can get the further pictures of magnetization reversal process. It's due to new numerical method application.

1. Hybrid boundary/finite element (high order FEM) method, like fig. 2.3.1, basic micromagnetic processing for polycrystalline Co element [17].

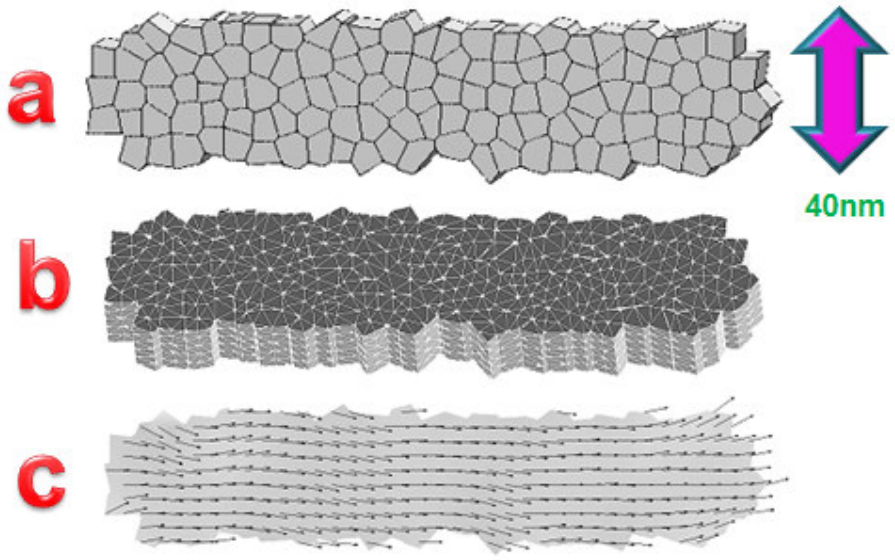

Figure 2.3.1 (a) Polycrystalline Co element in size of 200 x 40 x 25 nm^2 (b) Discretization of the element by finite element method (c) Magnetization ripple structure for zero applied field [24]

2. Advanced adaptive meshing technique. Now, even accurate stray field computation for any complicated shaped particle is available and it is also able to take granular microstructure into consideration by using periodic boundary condition.

Here, we can just give a simply introduction of micromagnetic development history. A continuous magnetization vector is originally used to present the transition region of domain, by Brown, 1963. It is no more used to take account of the individual atomic moments. The traditional reversal mechanism of small ferromagnetic particle assumes particles magnetize uniformly along easy axis. This is a process for magnetization deviate from equilibrium state, basing on preferred magnetization mode, by Frei 1957, and Aharoni 1962. Many different numerical methods, like FEM (Koegler 1992) and FDM (Schabes 1988, Nakatani 1989) are applied in reversal mechanism studying in non-ellipsoid particles. Victoria 1988, Yan 1988, Schabes 1991 showed that the reversal process will be influenced due to the large stray field causing the magnetization inhomogeneously arranged. Then, the effects of magnetostatic and inter-grain exchange interaction on remanence and coercivity for an isotropic model magnet composed of cubic were studied

by Fukunaga and Inoue, 1992.

Thanks to the advanced computational architecture in 1998, the dynamic motion by the finite element method in 3D system can be demonstrated by new numerical procedures, Yang and Fredkin. The dynamic motion is commonly describe by the Landau–Liifshitz–Gilbert (LLG) equation. The following fig.2.3.2 illustrates the damping gyromagnetic precession motion. In this study, the spin transfer torque (STT) will not be taken into consideration.

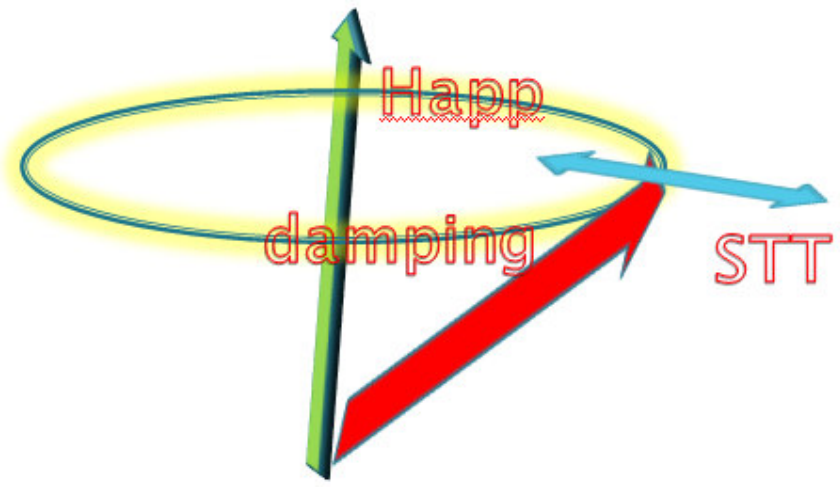

Figure 2.3.2 Damping gyromagnetic precession motion of a polarization vector J. The spin transfer torque is taken into consideration. STT term and damping are competing for energy equilibrium.

Some interesting topics in micromagnetic obtained more attentions

in other area. Boerner 1997, Chantrell 1998, Lyberatos 1993, and Nakatani 1997, they incorporate thermally activated magnetization reversal in simulation art. New hybrid micromagnetic models, including Monte Carlo method (Nowak 2000, generally used in nano particles case) is becoming more and more available.

The ordinary micromagnetc approximation has to be modified for some special cases, proposed by Chubykalo-Fesenko, in 2006 publication. He showed [25, 26] the micromagnetic method maybe fails, when dealing with a soft/hard bilayer system with a large spatial variation of the exchange coupling.

The reason is that [25, 26], micromagnetic modeling allows huge spatial variation of magnetization, since it underestimates the accompanying exchange energy. In this case, this atomic and multi-scale models taking into account exchange is important.

The basic difference between these two modeling is described as following. The atomic level modeling uses a suitable physical model for the exchange, unlike the micromagnetic approximation of long-wavelength. The references [27, 28] are calculated based on atomic level.

The following fig.2.3.3 and fig.2.3.4 illustrate a standard meshing process for finite element method in micromagnetic and standard meshing model for 3D cubic particles. The fig. 2.3.5 is another meshing

method, multi-scale method.

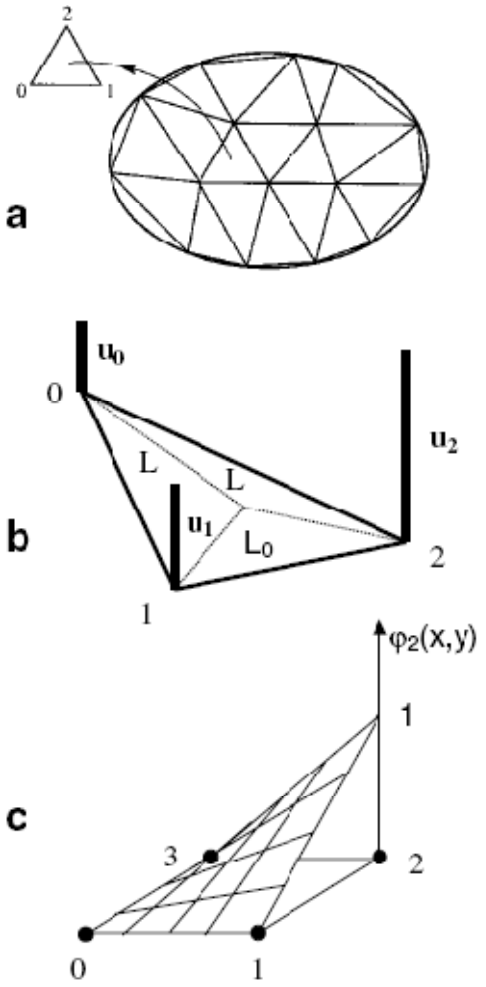

Figure 2.3.3 (a) Triangulation into finite elements for a 2D domain. (b) In the region contained in nodal points 0, 1 and 2, use a linear function for interpolation. (c) Shape function $\varphi_2(x, y)$ for a quadrilateral. [24]

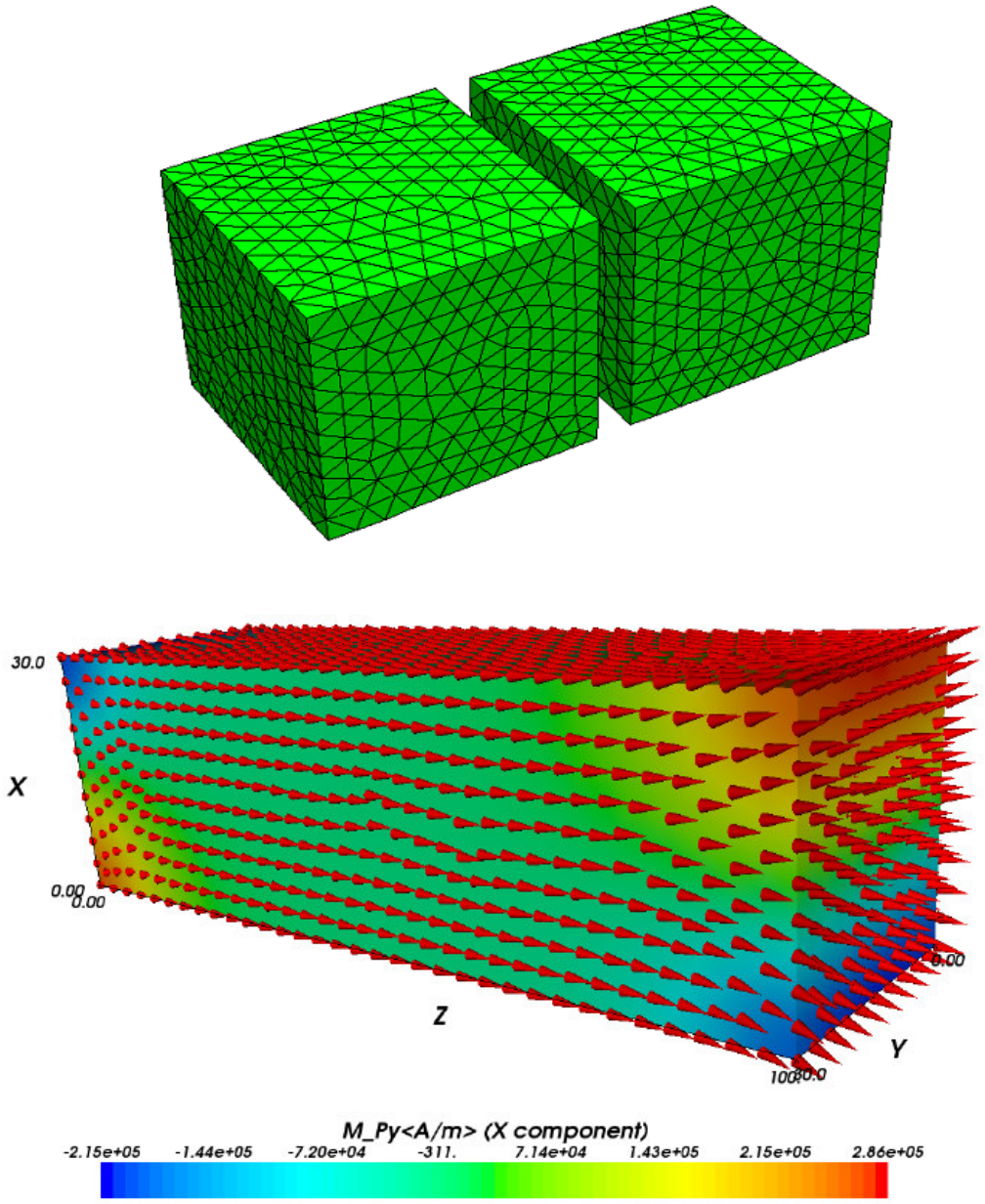

Figure 2.3.4 Two meshing cubic particles. Generated by nMag micromagntic simulation package (upper) and micromagnetic solved magnetization distribution in below (http://nmag.soton.ac.uk/n mag/)[62]

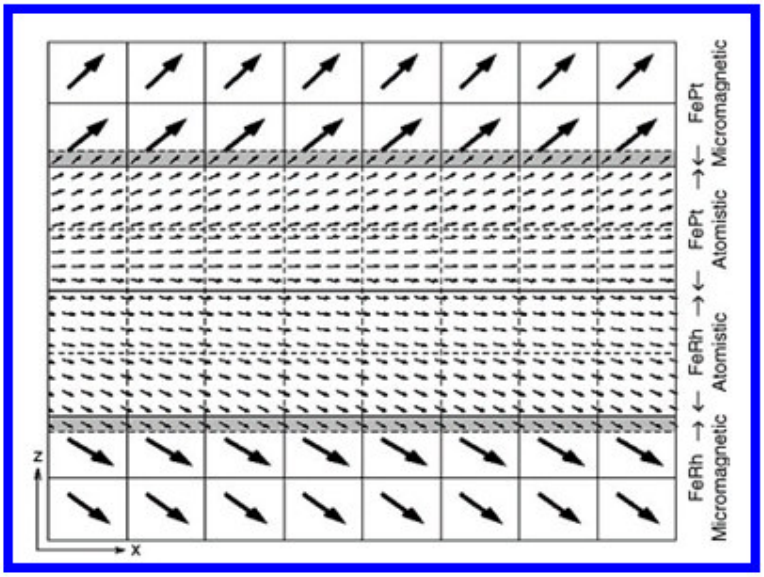

Figure 2.3.5 The multi-scale modeling mesh structure [26]

2.4 ECC, exchange spring, and graded media system

We all know that the higher recording density is always sought by advanced recording technology. So the decreasing of grain size is required to maintain an ideal signal-to-noise ratio (SNR). But a new problem comes as following. The thermal stability could be decreased due to a smaller energy barrier of a smaller grain size. This effect is known as superparamagnetic limit. It happens as the thermal fluctuations lead to switch the magnetization spontaneously.

For a small size magnetic particle, the term "K×V" is theoretically considered as the energy barrier for thermal induced switching. It is also obvious that the grain size reduction can be balanced by the enhancement of anisotropy.

Of course, the thermal stability issue can be improved by feasible material selection. FePt possesses the high magnto-crystalline anisotropy, with constant of order $7e^6$ J/m^3. It is much better than other common used Co-base alloy. But in the case of large anisotropy, the maximum writing field is a new challenge which cannot be neglected.

Magnetization also decides the switching field value, like following,

$$\mu_0 H_c = 2K_1/M_s$$

But the accompanying increase in demagnetization field also should be taken into consideration. There are really some "trade off" between stability, grain, anisotropy, and write head fields.

A novel media model was proposed by Victora and Shen [29], containing a soft layer and one hard layer. The "soft" and "hard" describe the low and high anisotropy for each layer. Many previous studies indicate this media model can reduce the switching field, comparing to a single layer film structure. This is because the soft layer can be reversed first and then it induces the reversal of the hard layer. The bottom hard layer, it can provide the required stability. It is so-called exchange coupled composite media (ECC media).

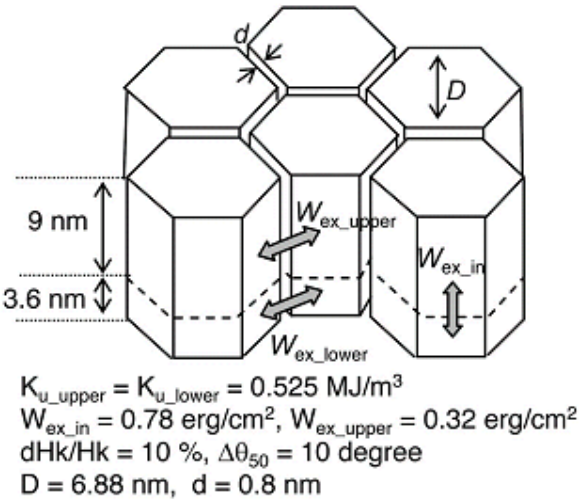

Figure 2.4.1 The micromagnetic modeling of hard/soft bilayer granular system [30].

The basic property for bilayer system can be described to have average magnetization and anisotropy as following, where M_{eff} is the average magnetization, and $\mathcal{I}_{hard}$ and $\mathcal{I}_{soft}$ are the thickness of hard layer and soft layer, respectively.

$$M_{eff} = (M_{hard} \times \mathcal{I}_{hard} + M_{soft} \times \mathcal{I}_{soft})/(\mathcal{I}_{soft} + \mathcal{I}_{hard})$$

$$K_{eff} = (K_{hard} \times \mathcal{I}_{hard} \times K_{soft} \times \mathcal{I}_{soft})/(\mathcal{I}_{soft} + \mathcal{I}_{hard})[31]$$

And the energy barrier can also predicted as,

$$\Delta E = K_{eff} \times F + (\mathcal{I}_{soft} + \mathcal{I}_{hard})$$

This is a relatively simple case, where the ratio $\Delta E/H_c$ is determined

by the average magnetization and grain size value.

But the latter simulation work by Suess [32] shows that the above homogeneous reversal assumption is not the real case for bilayer system consisting of exchange coupled soft and hard layer. This novel type media is called an “exchange spring” media. This mechanism is similar to the compose permanent [33]. As an external field increasing, the soft layer with small Ku value will start to reverse its magnetization, and then acts as a spring to initiates the hard layer reversal. Magnetization reversal configuration is show in fig. 2.4.2. It has been reported due to this mechanism [34, 35], with a zero anisotropy soft layer, the bilayer structure Hc can be reduced to one quarter of the anisotropy field.

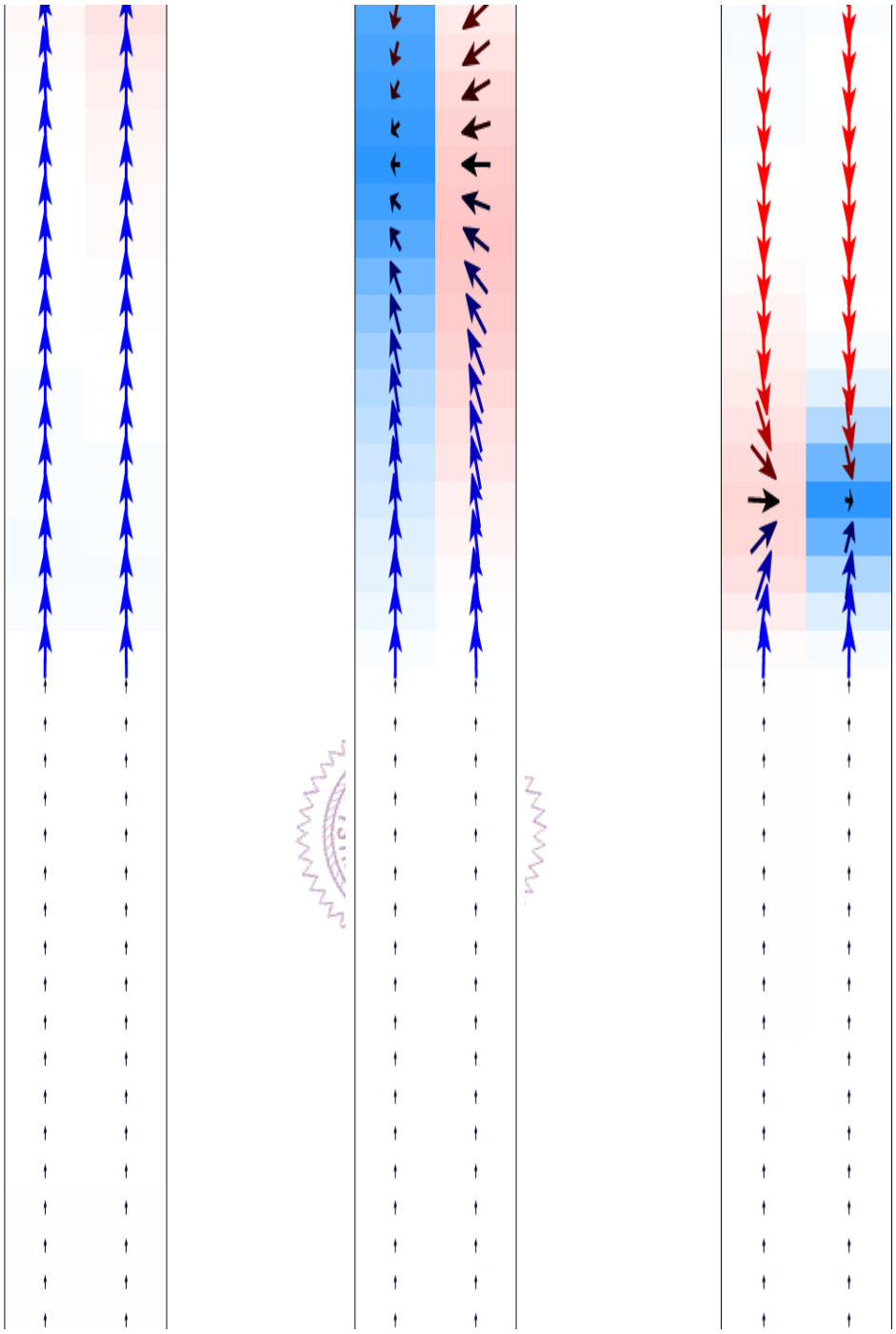

Figure 2.4.2 Magnetization reversal configuration by OOMMF code [36]

Detailed micromagnetic simulation indicates that, as the external field reaches Hc value of soft layer, the domain wall forming at the interface between the hard and soft layers propagates into the hard layer. The thickness of the soft layer in exchange spring plays an important role in the reversal mechanism. Because for thermal stability concern, the thickness decides which reversal model is preferred, homogenous rotate or non-homogenous mechanism.

Not only in the soft layer, there is also a critical thickness for hard layer. That is the optimum hard layer thickness can adjust the homogeneous reversal to have the same energy barrier as the domain wall energy for hard layer.

For exchange spring mechanism, the transverse procession in the interface between soft and hard layers rises many analytic studying. The following Fig. 2.4.5 presents two layer phase boundary. Soft and hard layer have their own properties. In this simplified case, only spontaneous magnetization J_S , anisotropy constant K_l , exchange constant A will be taken into consideration. In some previous work [37], their first step of analysis is to calculate domain wall energy in boundary. Then minimize φ with respect to φ_1 and φ_2, in addition with bound condition. Solving the equation $\frac{dH_{ext}}{d\varphi_0} = 0$ under an external field applying, leads the pinning field form as,

$$H_c = 2\left(\frac{K_1^{II}}{J_S^{II}}\right)\frac{1-\epsilon_K\epsilon_A}{(1+\sqrt{\epsilon_K\epsilon_A})^2}$$

This is very obvious that the boundary pinning field must be always smaller than the nucleation field of the second phase (hard layer).

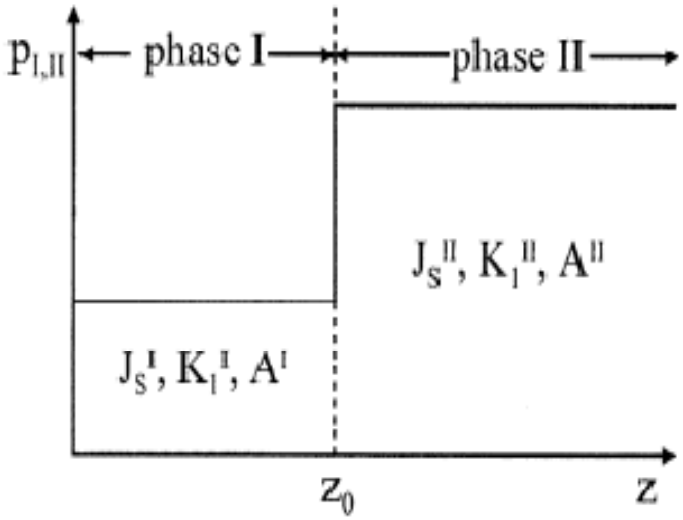

Figure 2.4.5 Two materials phase boundary [37].

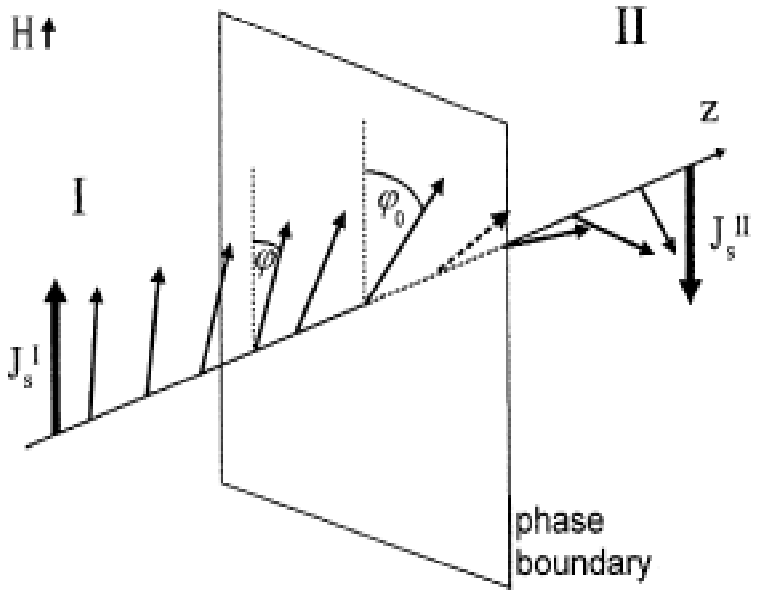

Figure 2.4.6 Domain wall spin configuration under an external field [37].

It has been shown that the ultimate potential of exchange spring media can be realized when the interfacial domain wall fits inside the soft and hard layers [38]. The ratio of the energy barrier over the coercive field can also be modified. Suess indicates that [39], due to the different reversal model of the field–induced switching process, the ratio of the energy barrier over the coercive field can be optimized by the magnetic properties of the bilayer structure .

The difference between exchange spring media and ECC media is the reversal mechanism in soft layer. One is uniform rotation, and the other is noncoherent dynamic rotation. Noncoherent dynamic rotation only occurs in the case of thicker soft layer, in which the thickness of the soft layer is larger than the domain width.

On the other way, the normal method in order to get the uniform rotation in micromagnetic, sometimes called the infinite exchange model, is to set value of exchange to a very large value. It forces all the magnetization vectors to point in the same direction.

Three different nucleation models are usually discussed based on micromagnetic, derived from the numerical micromagntic method. The following fig.2.4.7 illustrates the homogeneous rotation, curling, and buckling [40].

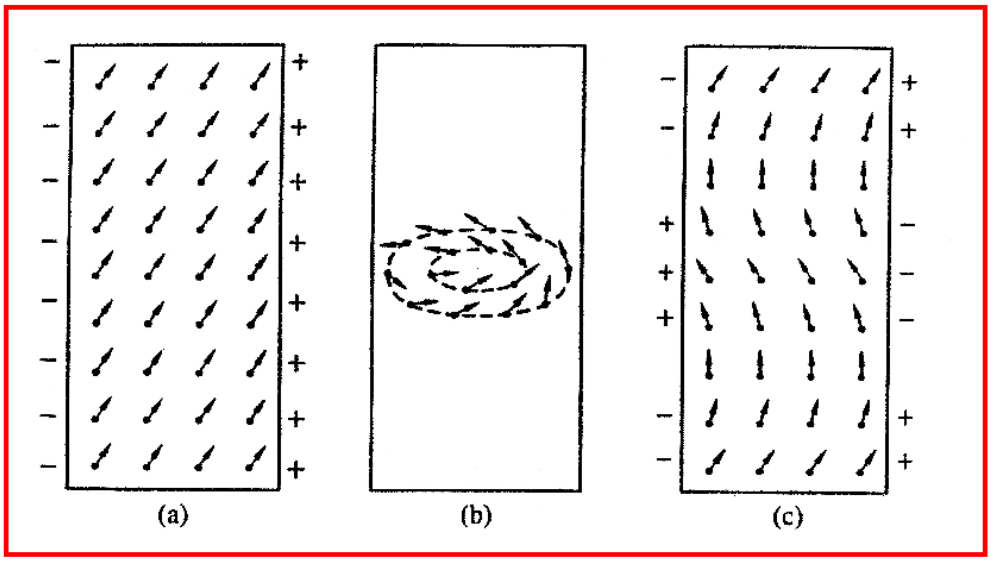

Figure 2.4.7 The homogeneous rotation, curling, and buckling [40].

And twice the exchange length, $2R_0 = (\frac{2}{M_S})\sqrt{4pi/\mu_0}$, which is considered to be the limit between coherent rotation and inhomogeneous reversal processes, is the upper bound for the column length in

perpendicular recording media[41]. In other words, this kind of reversal model is energy-favored.

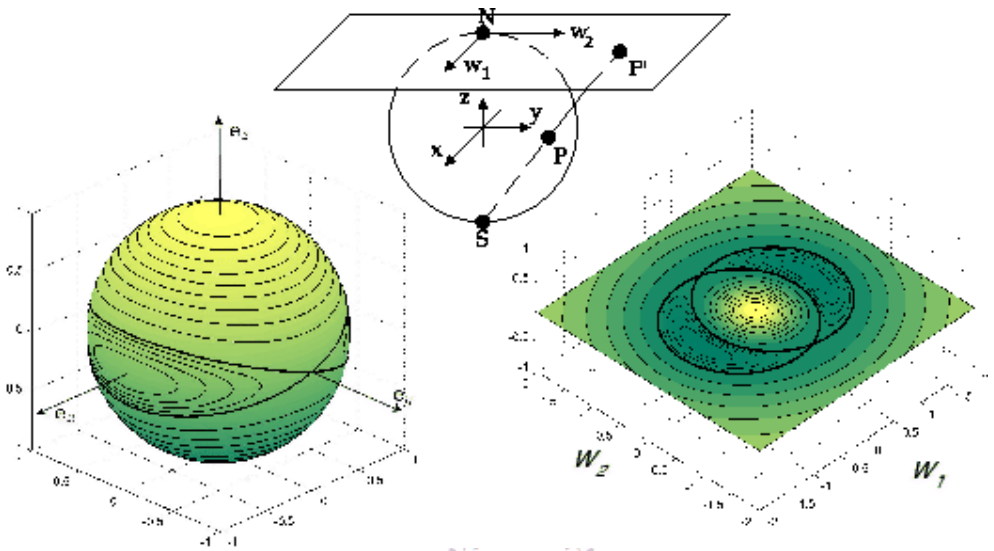

Figure 2.4.8 Stereographic projection of the unit-phase on the plane [42].

For the composite media, angular dependence of coercive field is strong related to the signal to noise ratio [43]. The common formula is described in Stoner-Wohlfarth theory as $H_C = 2K_1/J_S\gamma(\theta)$, especially suitable for domain wall pinning control material. Generally speaking, the 5% deviation between analytic method and finite element based micromagnetic approach is acceptable. Moreover, composite media is less affected by angular dependence effect than single layer due to different energy barrier. Previous study [32] shows for 10 degrees misalignment between external field and the easy axis, the resulted Hc value will be increased by a fact of 1.01 and decreased by 0.68 for each one.

H. Kronmüller, D. Goll neglect the demagnetization field in their study, with two hard/soft layers for parallel easy axis direction. Based on the assumption that polarization and the exchange constant are the same in both layers, a formula valid for infinite thick hard and soft layer is simplified to

$$H_c = (2K_{l,hard} - 2K_{l,soft})/4J_s$$

In this formula, we can prove that if the soft layer is of zero anisotropy, the Hc value of hard layer can be lowered to a factor of four as mentioned previous. Guslienko et al. [28] investigate limit of strong and weakly exchange coupling bilayer system nucleation and switching field.

$$H_{SW}(T) = -H_{al}(T) + \frac{J_{12}}{d_1} M_2(T) \times \left[1 + \frac{J_{12}}{L} \frac{M_1(T)}{(H_{al}(T) - 4piM_2(T))} \right] \quad (a)$$

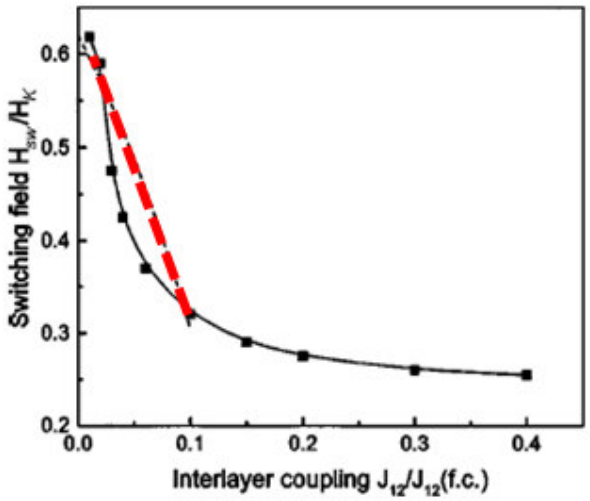

Figure 2.4.9 In FePt/FeRh bilayer, the switching field is plot corresponding to different interlayer coupling $J_{12}/J_{12}(\text{f.c.})$. The red dashed line is the solution of Eq. a

Kronmüller and Leineweiber [44] calculated the nucleation field of trylayer system (hard/soft/hard) in the limit of strong interface coupling interaction. In the case of hard magnetic phase, the exchange coupling is completed, and magnetization reversal takes place by homogeneous rotation. This phase is dominating if soft layer thickness is smaller than approximately the hard layer Block wall thickness. It is also demonstrated a strong influence of the soft inhomogeneity size on the nucleation field for exchange coupled phase. This kind of magnetization reversal occurs collectively as inhomogeneous rotation. So any point of the sample at field below the nucleation field will spread throughout the whole sample. In decoupled phase, the different nucleation fields are obvious. And the reversal for each layer takes place irreversible and independently.

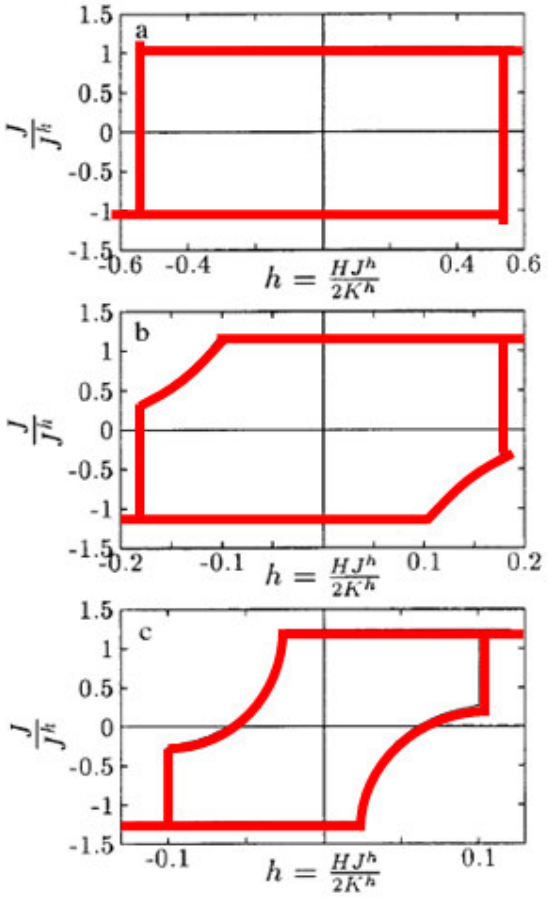

Figure 2.4.10. Three kinds of hysteresis loop. (1) hard magnetic phase with soft layer thickness of 2.1nm; (2) exchange coupling phase with soft layer thickness of 6.3mn; (3) decoupled phase with soft layer thickness of 11.3nm.

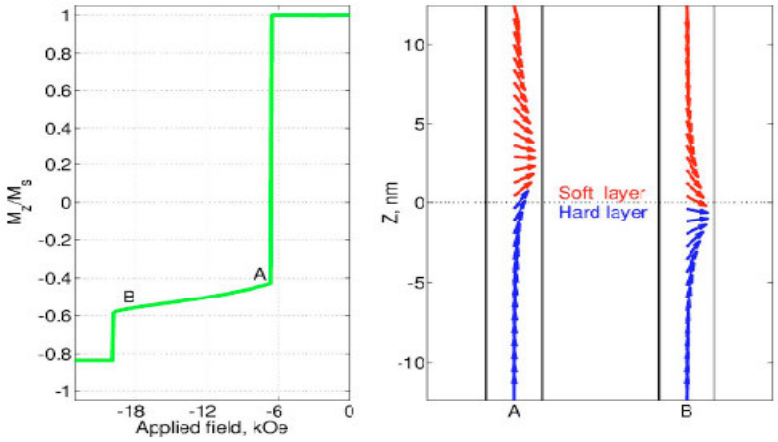

Figure 2.4.11. MH loop and dynamic moment tilting distribution in composite media [45].

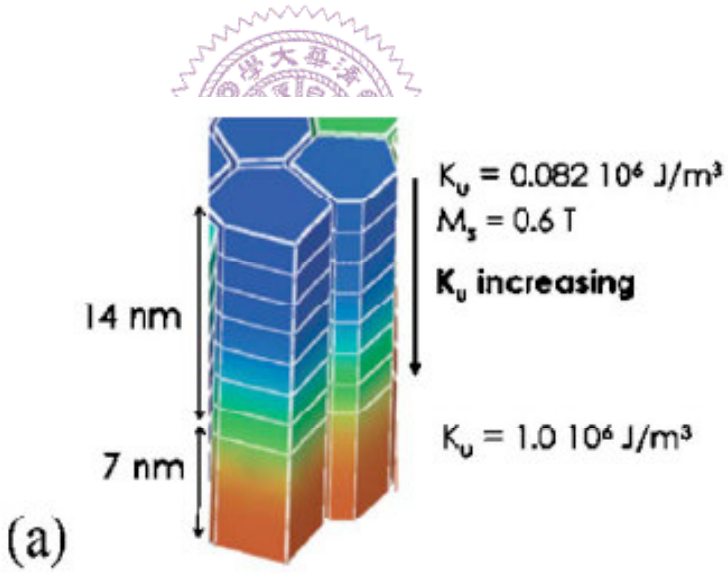

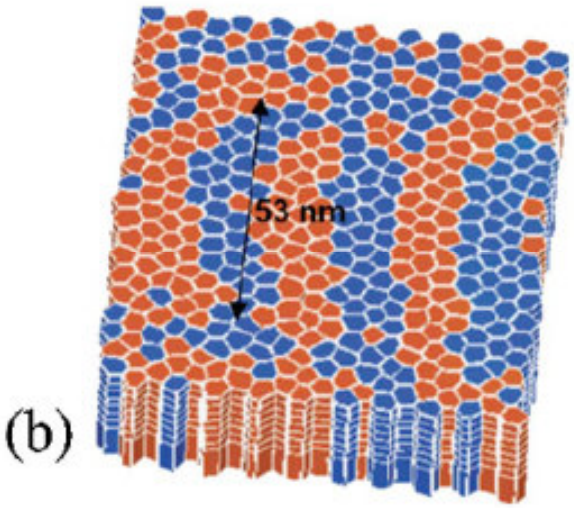

Figure 2.4.12. 1 T bit /in^2 simulation in graded media system [46].

Chapter3 Experiment design and simulation model

3.1 Experiment Flow Chart

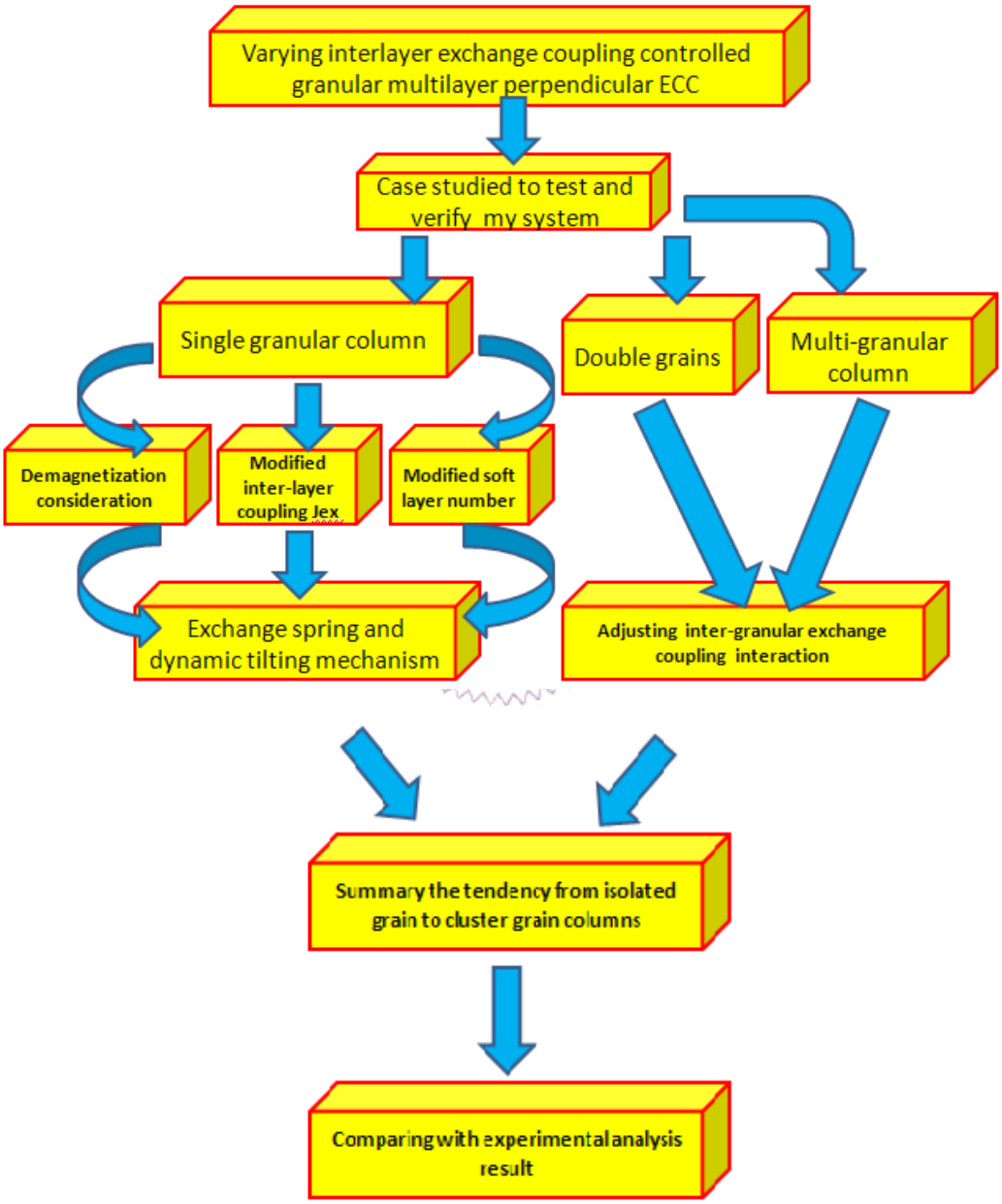

3.2 Software and Numerical Micromagnetic model

The OOMMF code is modified at 3 specific levels. For the top level, individual programs interact via well-defined protocols across network sockets. User can connect these modules together in various ways from the user interface, and new modules speaking the same protocol can be transparently added as well. The second level of modification is at the Tcl/Tk script level. Tcl/Tk scripts is allowed to be imported and executed at run time for some modules, and the top level scripts are relatively convenient to adjust for specific purpose. The lowest level is based on the C++ source code. The OOMMF extensible solver, OXS, is designed with modification at this level in mind.

Some standard numerical methods are used there, such as minimum energy method, Euler method, and Runge-Kutta method. For each applied field, the evolution of the spin system is calculated by the LLG equation, until the maximum torque $|m \times h|$on the whole spin decays below a specific threshold value. This means the equilibrium magnetization of this external field is obtained. For the basic energy term, like exchange energy, is estimated by neighbor dot product approach [48]. The fast Fourier transform is introduced to calculate the magnetostatic potential which can be differentiated to get the magnetic field [49].

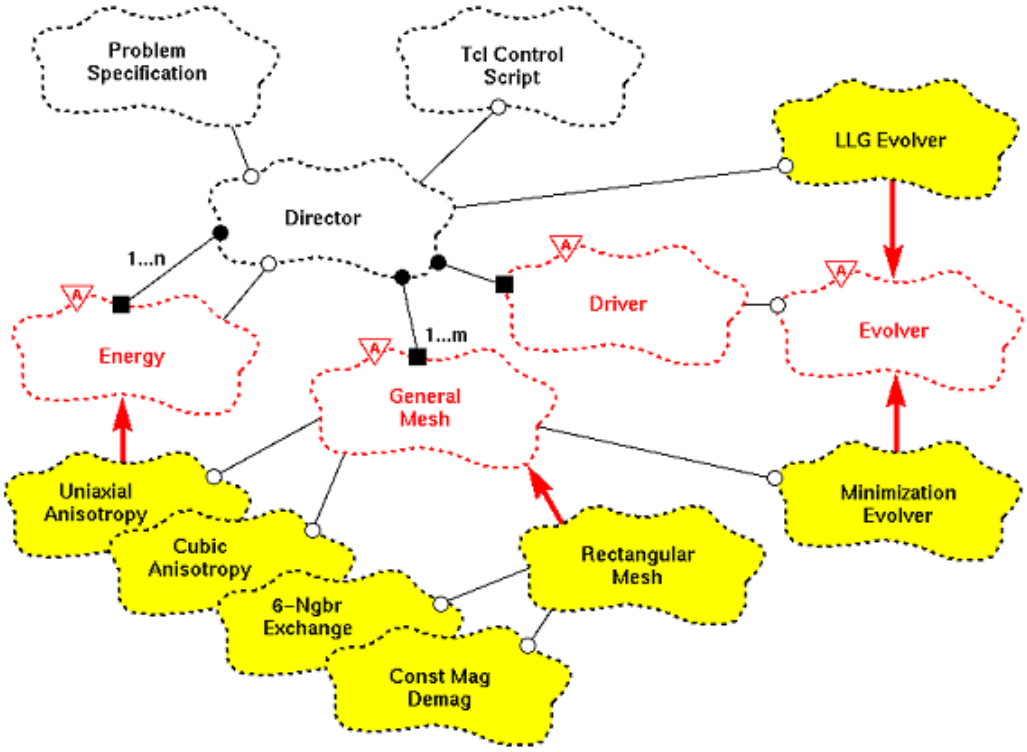

Figure 3.0 The OXS top level class diagram [50].

Chapter4 Results and discussions

4.0 Verify and test my simulation system

Here, we will test the reliability of our program by comparing with the previous study, “Domain wall assisted reversal mechanism”- Yu. Dobin and H. J. Richter, APL 89, 062512(2006)[51]

4.0.1 Introduction

This is a soft/hard bilayer coupled system, with an interfacial boundary constrain and one dimension infinite film thickness in the soft layer. The unit of applied field used in this chapter is m T (1 m T=10 Oe).

4.0.2 Result and discussion

At first, my conducted simulation performs the similar loop shape with the paper, but the value of switching field is much different. So I guess that, different in-plane domain size and meshing constructing lead to different switching field. There are two issues included. (1)This may be due to different magnetization for different cases. (2)Verify the in-plane condition.

To get the solution of this case, I neglect the demagnetization field. The case is set in an infinite geometry of the in-plane direction. It is just

like infinite planar capacitor board, the shield effect will eliminate the demagnetization field. Switching field gets closed to the paper case. Loop shape and reversal mechanism is also very similar. For paper, switch field (hard/soft) is 20kOe/6kOe. And for our case, switch field (hard/soft) is 19.5 kOe/6.4kOe. The detail is illustrated in the following fig. 4.0.1.

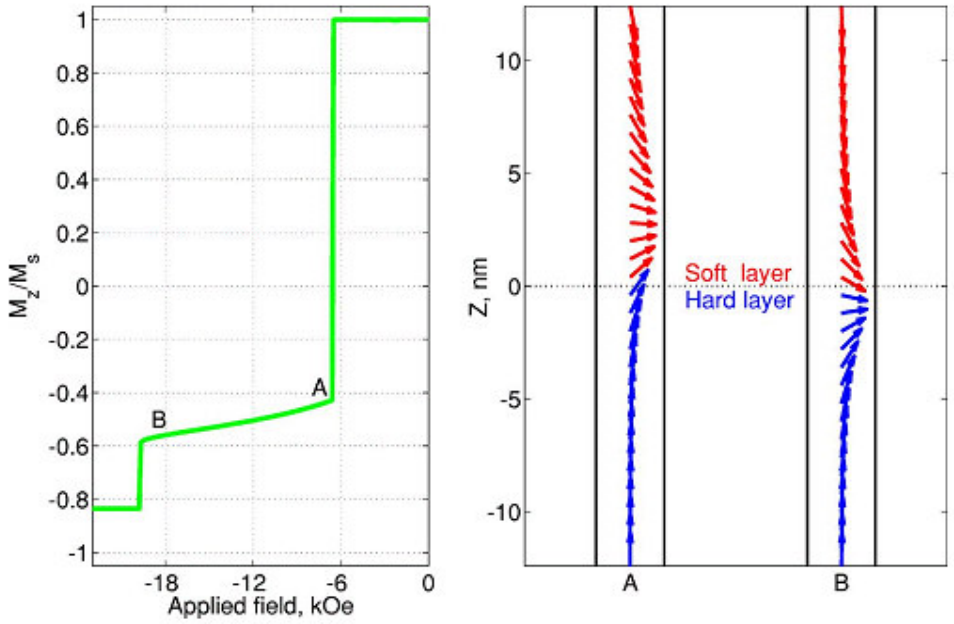

(a) **(b)**

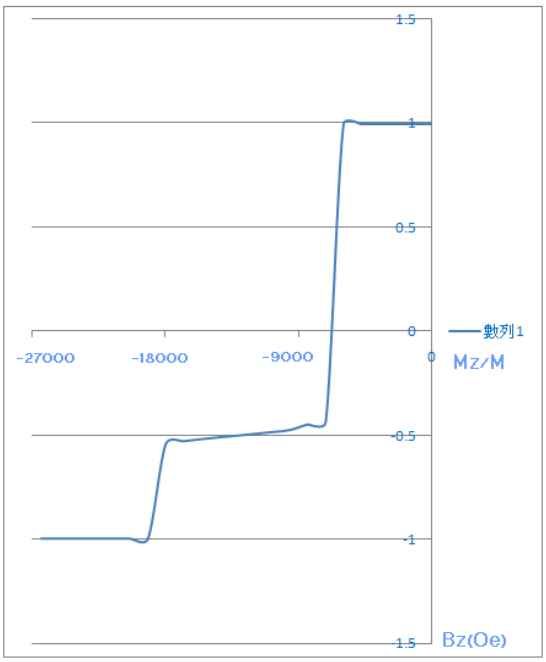

(c)

Figure 4.0.1 The demagnetization and spin configuration demonstrated by A. Yu. Dobin and H. J. Richter in APL [45] (a) and (b). Compare with my simulation work (c)

4.1 Demagnetization field fact in single grain system

4.1.1 Introduction

Demagnetization field (H_d) is induced by the external applied field inside the magnetic body, with a direction opposite to the external field. This kind of phenomenon actually eliminates the external field. In the past several decades, numerous methods are developed for demagnetization calculation. It can be described as a form, where the N_d is the demagnetization factor.

$$H_d = N_d M$$

Notice that the H_d also has a magnitude inverse proportional to the distance between the magnetic pole. In this elongated shape of grain, the demagnetiation field can induce a shape anisotropy, demonstrated as following equation,

$$K_{shape} = \frac{1}{2}\ \mu_0 M_S^2 (n_x - n_y)$$

Another effect of H_d is proposed [39]. The magnetization of fully saturated media prefers the reversal of individual grain, if only the H_d is larger than the external field. Here, the H_d is calculated through the rectangular mesh in finite different method. And the Fast Fourier Transform is applied to compute the demagnetization field. The demagnetizating factor in the z-axis, D_Z, is defined as the factor making the magnetostatic self-energy per unit volume equal to $2piD_Z M_s^2$. The derived equation of D_Z and the corresponding coordinate system is shown in fig. 4.1.1 [47].

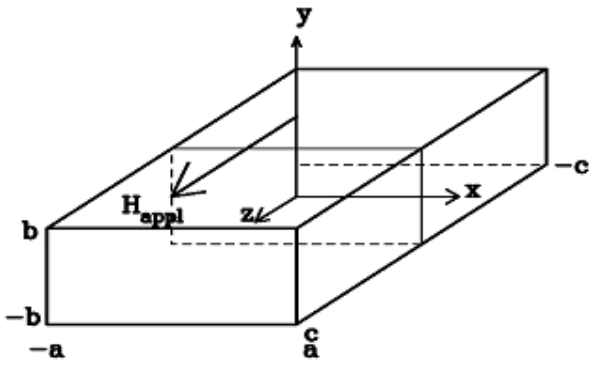

(a)

$$\pi D_z = \frac{b^2-c^2}{2bc}\ln\left(\frac{\sqrt{a^2+b^2+c^2}-a}{\sqrt{a^2+b^2+c^2}+a}\right) + \frac{a^2-c^2}{2ac}\ln\left(\frac{\sqrt{a^2+b^2+c^2}-b}{\sqrt{a^2+b^2+c^2}+b}\right) + \frac{b}{2c}\ln\left(\frac{\sqrt{a^2+b^2}+a}{\sqrt{a^2+b^2}-a}\right) + \frac{a}{2c}\ln\left(\frac{\sqrt{a^2+b^2}+b}{\sqrt{a^2+b^2}-b}\right)$$

$$+ \frac{c}{2a}\ln\left(\frac{\sqrt{b^2+c^2}-b}{\sqrt{b^2+c^2}+b}\right) + \frac{c}{2b}\ln\left(\frac{\sqrt{a^2+c^2}-a}{\sqrt{a^2+c^2}+a}\right) + 2\arctan\left(\frac{ab}{c\sqrt{a^2+b^2+c^2}}\right) + \frac{a^3+b^3-2c^3}{3abc}$$

$$+ \frac{a^2+b^2-2c^2}{3abc}\sqrt{a^2+b^2+c^2} + \frac{c}{ab}\left(\sqrt{a^2+c^2}+\sqrt{b^2+c^2}\right) - \frac{(a^2+b^2)^{3/2}+(b^2+c^2)^{3/2}+(c^2+a^2)^{3/2}}{3abc}.$$

(b)

Figure 4.1.1 The derived equation of D_Z (a) and the corresponding coordinate system (b) in finite difference method (FDM) meshing calculations [47].

4.1.2 Simulation model detail.

Here, a multi-layer CoPtCr/SiO_2 with a hexagon basal plane single grain is involved in this simulation. The default damping constant αin LLG equation is 0.6, and the film structure is illustrated as well in the following fig. 4.1.2.

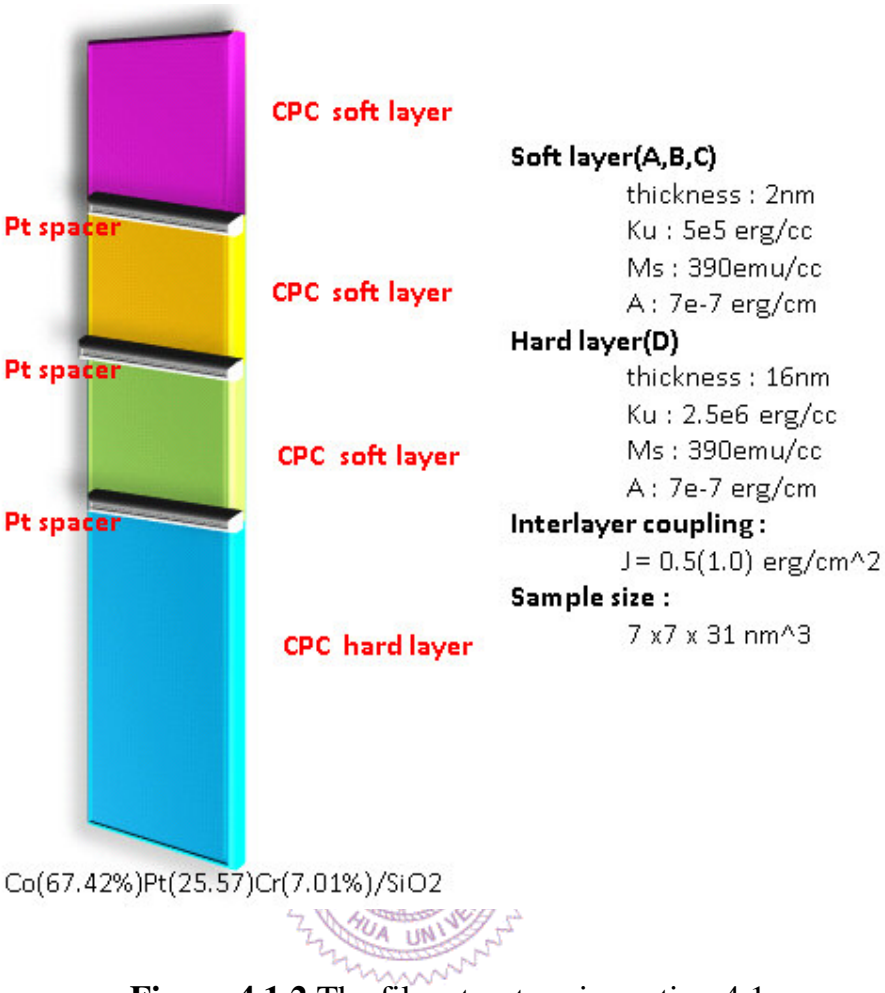

Figure 4.1.2 The film structure in section 4.1.

4.1.3 Results and discussions

According to the simulation result in fig. 4.1.3 we know that the demagnetization field will lead to a smaller switching field (or a nucleation field) within the single granular column, as well as a rapider switching process comparing with the case of non-demagnetization field.

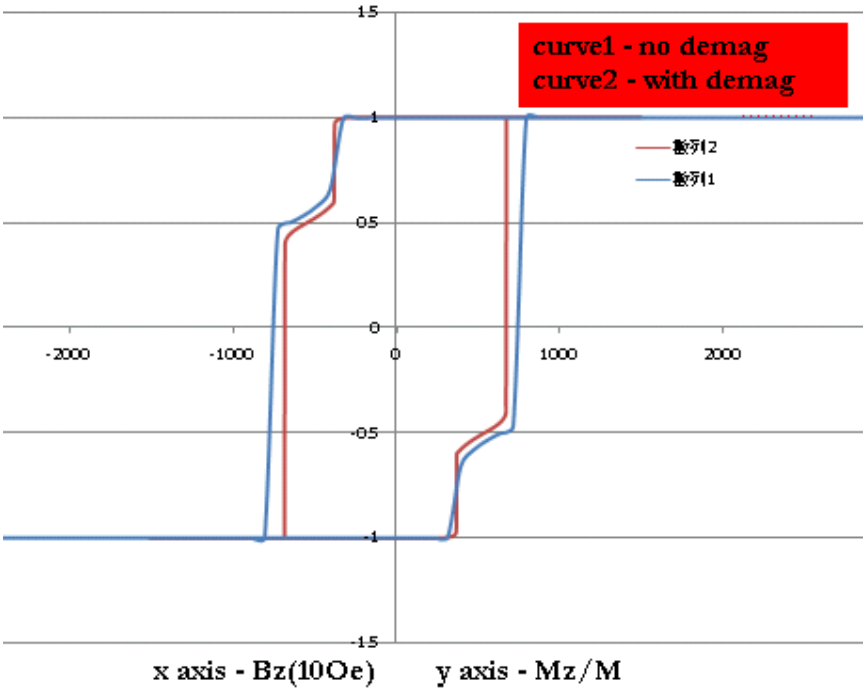

Figure 4.1.3 Hysteresis loops demonstrate the effect of demagnetization consideration.

It is highly approved that the demagnetization field affects the theoretical nucleation field (or switching) very deeply. Because the H_d induces a stray field, especially along the in-plane direction inside the grain. It tends to induce an unstable state of moment laying on the basal plane. When H_d gets involved, moment is more difficult to lay down in-plane from an initial out-of plane direction. So nucleation field increases. But it is easier to escape the in-plane direction when external field keeps increasing, so the slop is steeper.

Fig.4.1.4 indicates the continuous demagnetization varying distribution during the multi-layer reversal period. It is obvious that the

H_d within the upper soft layer first switching to the positive z-axis direction. This transition ends up with all the H_d heading in the positive z-axis direction after the whole reversal.

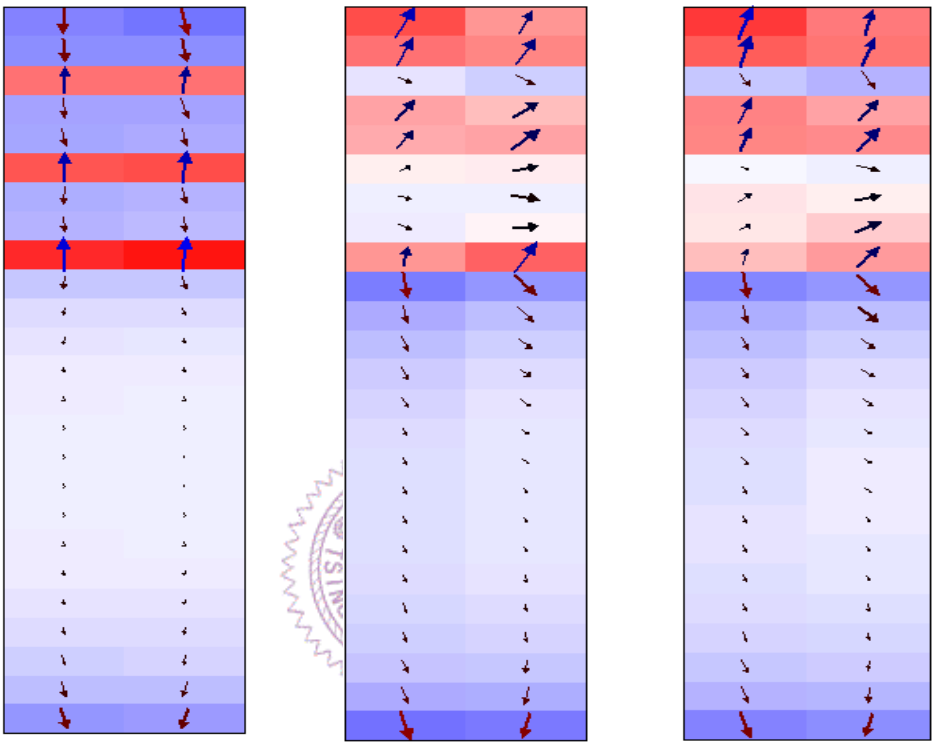

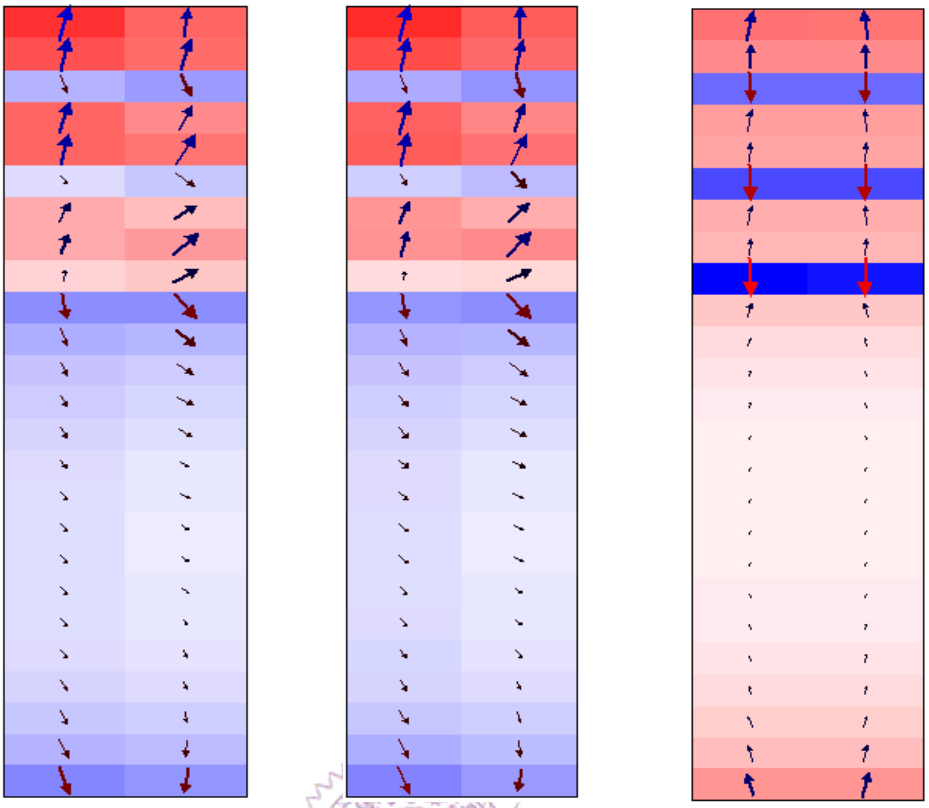

Figure 4.1.4 Demagnetization field inside the grain, at external field during the critical reversal period. The fields here are equal to -320, -400, -480, -640, -720, -800(m T). From the top left hand side to the bottom right hand side.

4.1.4 Conclusions

Two main issues involved with demagnetization field are the shape anisotropy and thermal stability concerns. With the present of demagnetization field, the strong in-plane stray field disfavors the moment lying on this plane. The magnitude of coercivity is therefore affected by this demagnetization field.

4.2 Modified inter-layer exchange coupling J in single grain system

The following simulation models in this thesis are all based on a relatively rougher zigzag-shaped basal plane. This kind of approach is set to make my modeling less time-consuming. This simplification makes sense because the in-plane shape anisotropy has less impact in out-of plane magnetization process.

In a normal exchange spring or ECC media, a magnetic soft layer is coupled with a hard layer. The major innovation of our design is the multi soft layer film structure, furthermore its magnetic properties can be controlled by film thickness and composition. By an appropriate control of exchange coupling interaction introduced in this film structure, the optima perpendicular anisotropy and magnetic performance can be achieved according to the micromagnetic analysis. It is exactly the issue this section aiming to study. This is so-called the ECC of varying interlayer exchange coupling control.

4.2.1 Introduction

.

The Pt spacer here can serve as an exchange spacer, and it controls the soft-soft layer exchange coupling strength which is reversely proportional to the Pt layer thickness. Some previous [51] studies have proposed that the Pt capping layer in Co/Pt/Cr system can improve the

SQ value and switching field distribution due to the Pt induced stronger perpendicular anisotropy and ferromagnetism of the thin Pt layer[52]. The Pt-Co interdiffusion can induce the ferromagnetism of Pt layer, which is able to contribute to induced perpendicular anisotropy. This phenomenon occurs in the Pt-Co interface for an ultrathin (smaller than 1.4 nanometers) Co layer thickness.

As an evidence for a mixed interface, the high electrical resistivity, enhanced magnetization, a diffuse Co compositional profile from XRD is strongly supported for this theory [52]. In more early periods, some literature [53] also claimed the similar case of ferromagnetic polarization of Pd atom by Co atoms in dilute Pd-Co alloy. The primary role of this coupling strength in the layer interface is addressed in the following discussion by different coupling strength.

4.2.2 Simulation model detail

The ECC media structure here has attractive advantages. Compared with what we called “graded media”, our system needn’t to change the material of soft layers. Only by adjusting the J value between soft layers, we can achieve the optimized reversal mechanism.

In this case, the detailed simulation parameter is as following, and the default damping constant α in LLG equation is 0.5. There film structure is set to approximately match our real experiment parameters, but some misfit is unavoidable due to the concern of computational

time-consuming issue (For our experimental parameter, soft layer thickness is 1.1 nm and spacer is 0.75nm). The model of film structure is presented in fig.4.2.1.

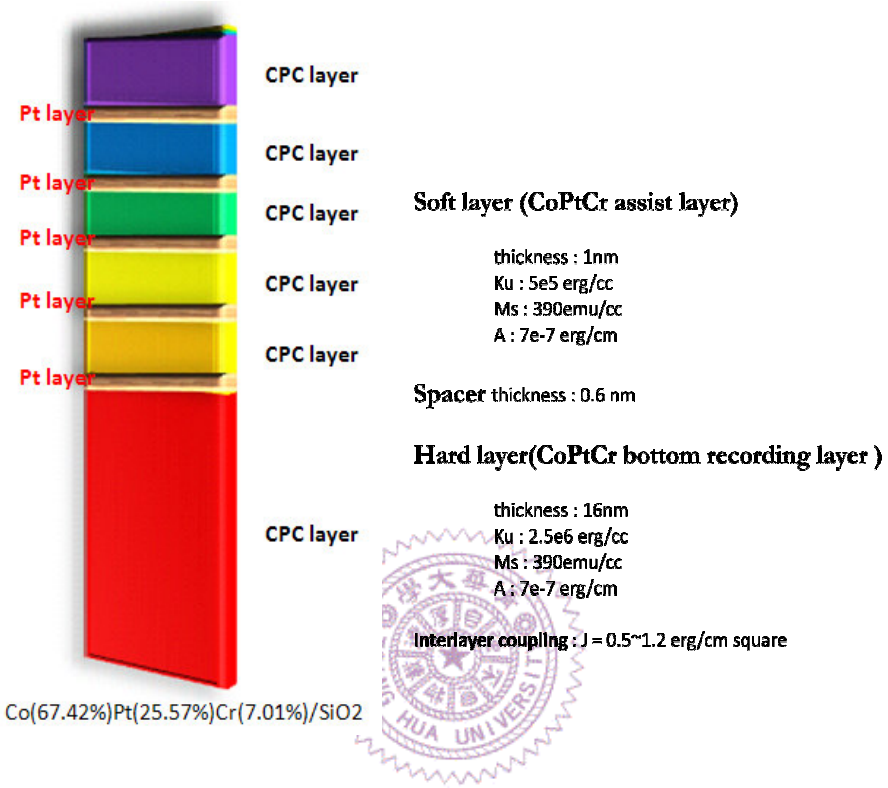

Figure 4.2.1 Simulation model detail in section 4.2 for film structure.

4.2.3 Results and discussions

In a typical exchange spring media, at the nucleation field, the magnetization state is very unstable with respect to creating a partial domain wall inside. We can denote the nucleation field and depinning field as H_n and H_{dp}, respectively. For $H_n < H < H_{dp}$, the loop could be some kind of round shape. The partial domain can be reversibly winded or unwinded. A further increase in the field completely reverses

the magnetization in soft layers such that it creates a domain wall contained both in the soft and hard layers. As long as the external field does not exceed the switching field, the domain wall can not be free to propagate and keeps pinned at the interface between soft and hard layers. When the external field exceeds the H_{dp} , all the layers, including hard layer magnetization can not resist the switching torque. So the full reversal of the whole sample is shown below. Actually, this kind of mechanism can be really observed by experiment [54].

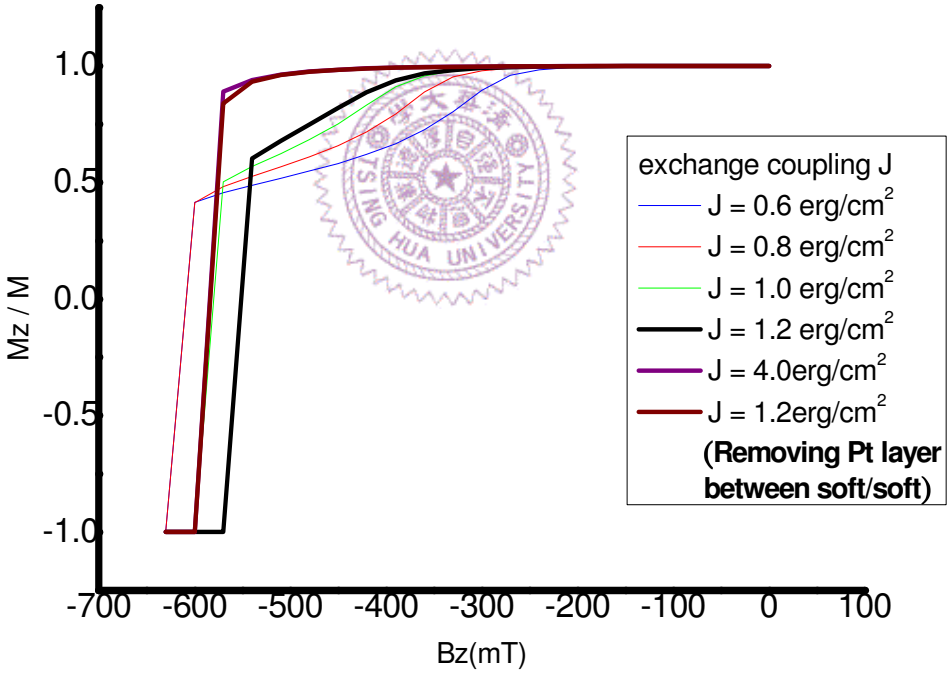

Figure 4.2.2 Hysteresis loops in the part of reversal processing with different inter-layer exchange coupling J values**.**

As external field increases, a series of reversed domain wall nucleates in soft layers. But every Pt inserted spacer served as a confine to limit the domain wall propagation length within each soft layer. This Pt spacer causes a pinning field to domain wall. As long as the external field exceeds the critical pinning field, the reversed domain expands through one specific soft layer and penetrates to the next one, and finally ends up in the fully reversed state.

According to fig.4.2.2, when the coupling strength is increased from 0.6 erg/cm^2 to1.2 erg/cm^2 , the coercivity decreases abruptly from 650 mT to 550 mT, but further increase to 4.0 erg/cm^2 in coupling strength induces the abrupt enhancement in the coercivity. We can make a brief summary from the discussion above. A sufficiently large J value (1.2erg/cm^2) is necessary, to maintain the stable state of each soft layer. But if this value is too large, it damages the domain wall propagation mechanism. Therefore the specific J value for optimum switching field reduction exists.

Previous work [53] in exchange spring pointed out that small interface coupling will cause a discontinuity of magnetization at the interface. Besides the switching field reduction also increases in proportion to the anisotropy difference between two coupling magnetic particles [55]. This kind of steeper loop indicates a sufficient torque between every soft/soft and soft/hard inter-layer coupling.

Experimentally, the coupling strength can be enhanced by reducing

the Pt layer thickness. But If the Pt layers between two soft layers are removed, the soft layers rotate coherently, due to their strong perpendicular anisotropy. And it leads to a larger switching field. It can also be proved that inserting the Pt layer really brings the batter magnetic property.

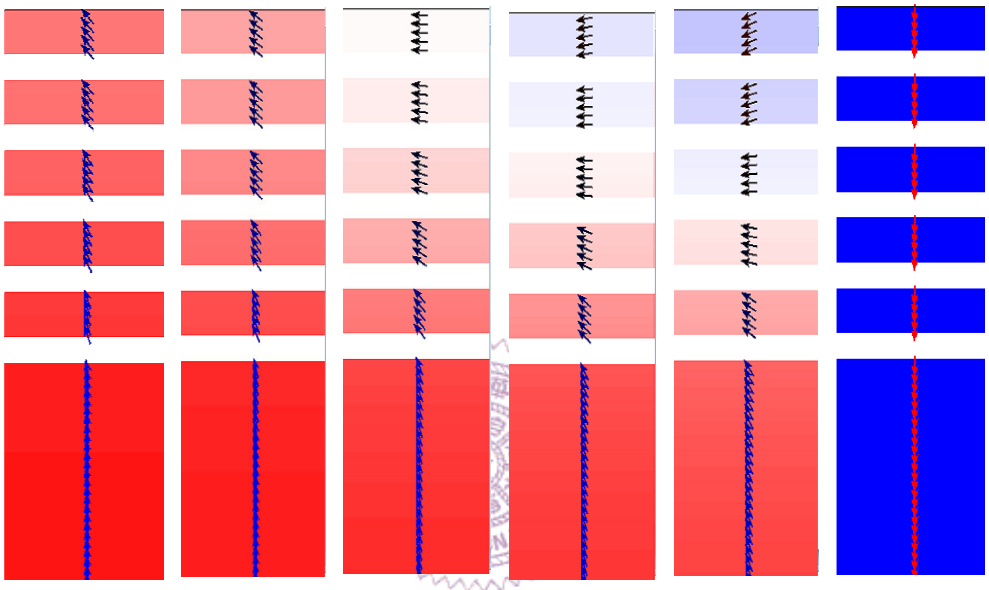

(a) spin configuration for J is equal to 1.2 erg/cm^2

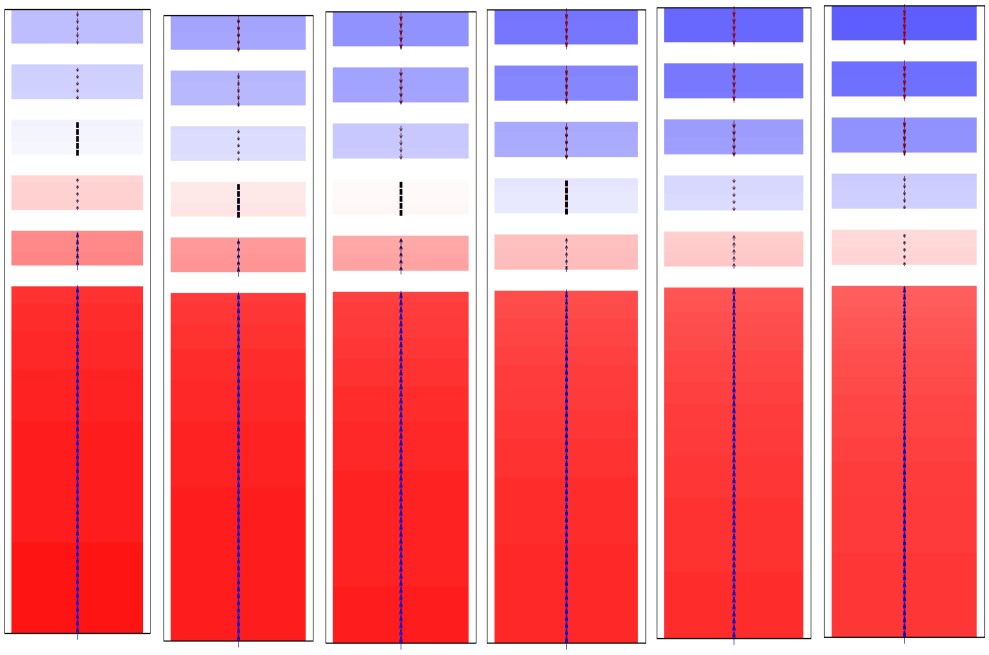

(b) spin configuration for J is equal to 0.6 erg/cm^2

Figure 4.2.3 The vertical spin configuration inside the grain during the reversal process. From left hand side to right hand side, they are external fields of -390, -420, -450, -510,-540 and -570mT.

Important messages from above spin configurations fig.4.2.3 should be emphasized are the distribution of the semi-domain wall to reversal mechanism. This means, the so-called domain wall assisted switching can not efficiently contribute in this case. The switching mechanism here is between the models of coherent and exchange spring.

The so-call exchange coupling density is defined as the energy between cell$_i$ belonging to layer$_i$ and its nearest cell$_j$ belonging to a layer$_j$. Here the layer$_i$ and layer$_j$are two neighboring soft layers. This concept can further provide a point of view from energy term to explain this mechanism. The energy across the spacer can be expressed as

$$E_{ij} = \frac{\sigma\left[1 - \mathbf{m}_i \cdot \mathbf{m}_j\right] + \sigma_2\left[1 - (\mathbf{m}_i \cdot \mathbf{m}_j)^2\right]}{\Delta_{ij}},$$

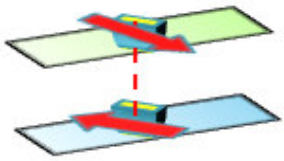

Where the σ is the bilinear surface exchange coefficient between the two surfaces, m_i is the normal unit spin at cell I, and the Δ_{ij} is the size of discretization cell. In fig.4.2.4, the energy path of J equal to 0.6

erg/cm^{2}and 1.2 erg/cm^{2}cases is shown.

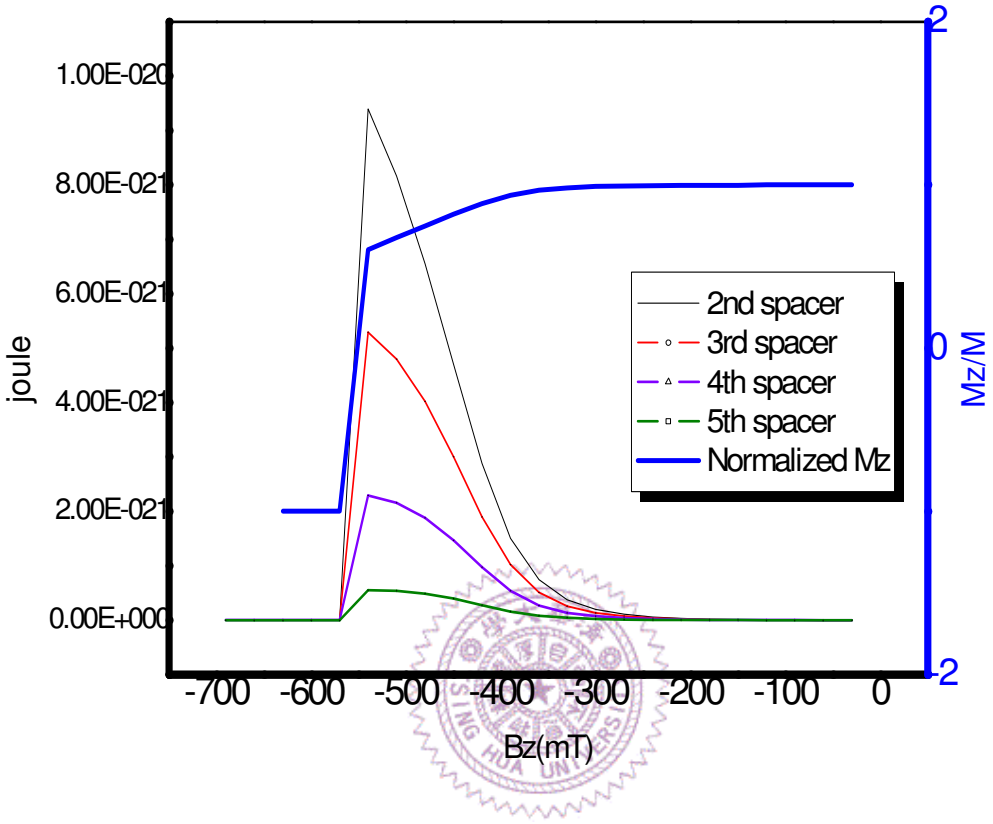

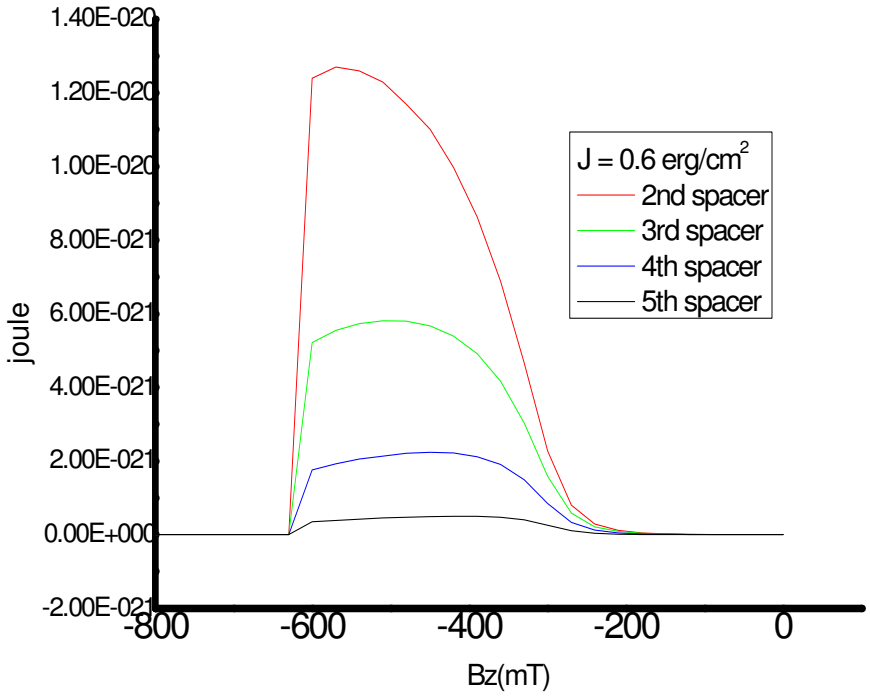

Figure 4.2.4 Inter-spacer exchange energy J is equal to 0.6 erg/cm^{2}and 1.2 erg/cm^{2}cases. Here the 2nd spacer means the spacer between 2nd soft layer and 3rd soft layer, and so forth.

The micromagnetic result shows the upper soft layer will take the lead in switching as the external field reaches the critical nucleation field. This kind of behavior gradually penetrates to the bottom soft layer as external field increases. This exchange energy simultaneously increases within each soft layer, and as these soft layers are more closed to the hard/soft interface, the exchange coupling energy will jump into a higher value. All the soft layers finish its switching process in the switching field, and each inter-spacer exchange energy abruptly decreases down to zero at this point, so the whole reversal state is obtained.

Fig. 4.2.4 shows a lower energy barrier of J equal to 1.2 than J equal 0.6. This means when J is equal to 1.2, the reversal can just overcome a relatively lower energy barrier. So the switching can be accomplished in lower applied field.

In fig.4.2.5, it is shown that under the condition of soft layer number n=5, J=1.2erg/cm^2, the semi-domain wall propagation can reduce the switching field from 10000Oe (for the plain hard layer) to about 5700Oe.

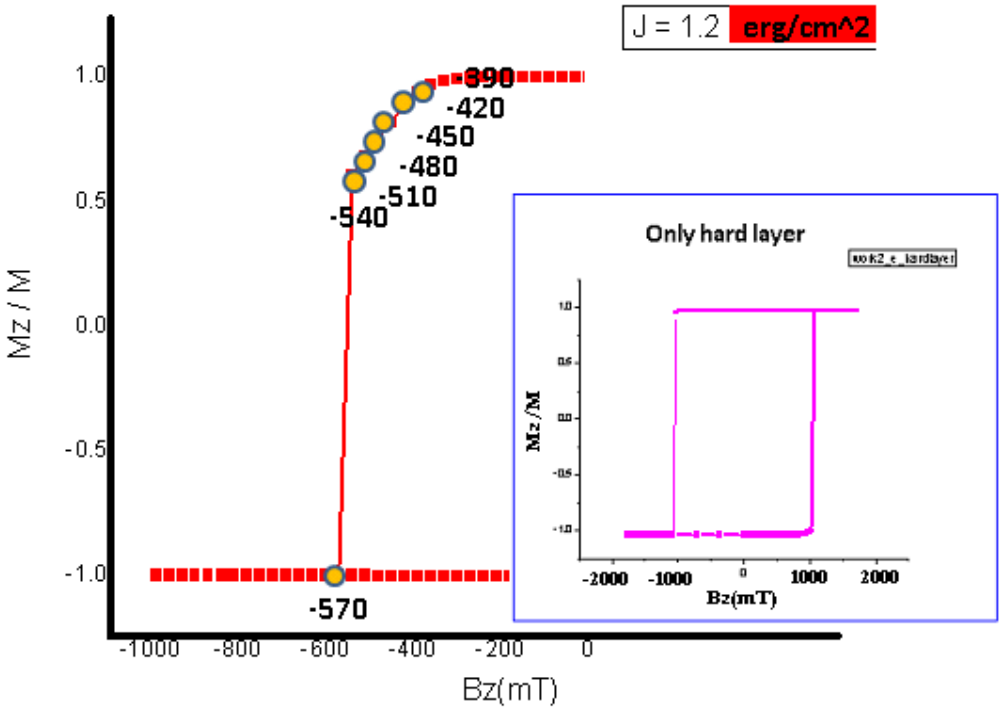

Figure 4.2.5 The simulation result matches the theory prediction. As the moment tilting in 45 degrees with the applied field in the soft/hard interface, the switching field of hard layer will decrease to half the intrinsic value.

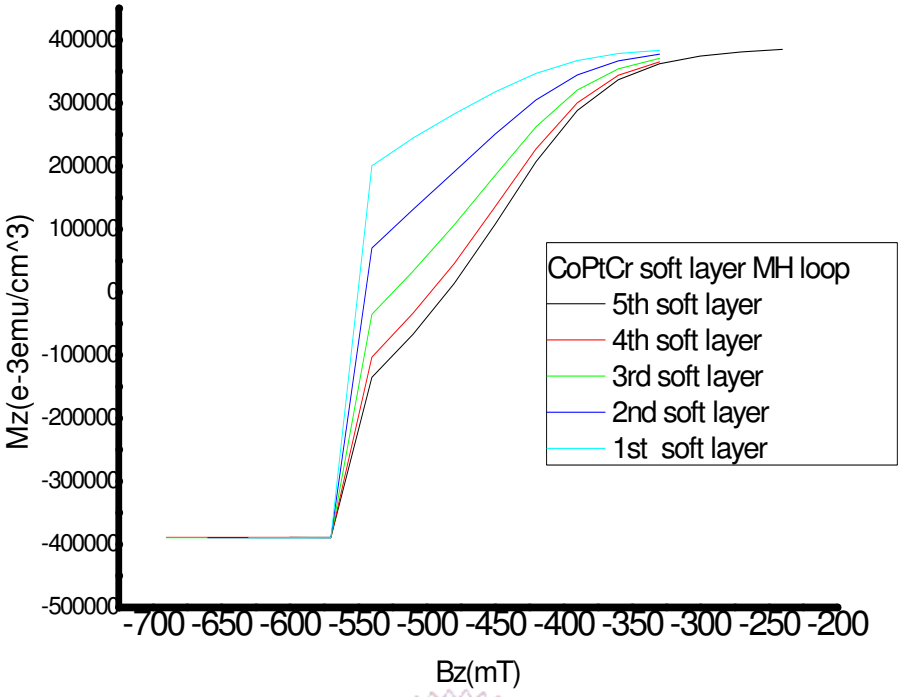

Figure 4.2.6 It is obvious that the toper soft layer reverses fist, and then the reversal mechanism penetrates into the bottom layer gradually.

The fig. 4.2.7 shows that the upper soft layers switch first and it applies torques to each successive layer. Some previous work [50] shows if the soft/hard layers exchange coupling is appropriate, the soft magnetization manages to torque the hard layer magnetization, resulting in flipping the entire grain.

4.2.4 Conclusions

The inter-layer coupling strength can strongly affect the magnetic property in this single grain model. An optimum J value can achieve a maximum reduced switching field. Micromagnetic simulation also shows

that inserting a non-magnetic Pt layer can successfully assist the magnetization reversal.

4.3 Soft layer number dependence

4.3.1 Introduction

It is mentioned previous, the spacer acts as a pinning site of domain wall propagation, and it confines the spin configuration. Enforce the spin nearby the spacer to lay in some specific specific direction, resulting in the spin deviation in this region. When the soft layer number increases, in other words, this loss will become intensive. The details are presented below.

4.3.2 Results and discussions

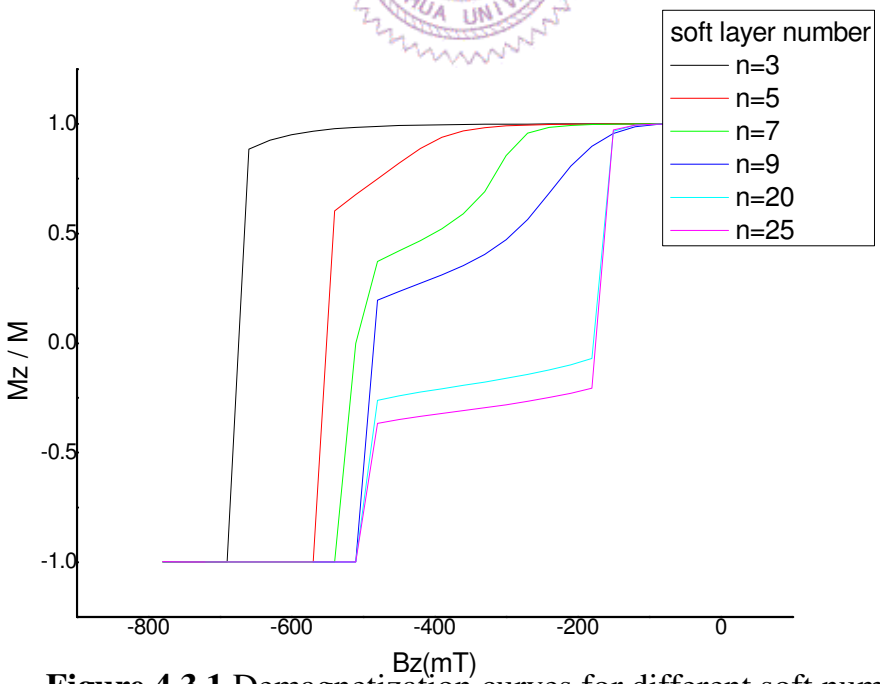

Figure 4.3.1 Demagnetization curves for different soft numbers.

The above simulation results reveal a terminal reduced saturation field when the soft layer number exceeds 9. The suitable explanation for this phenomenon is predicted to have something to do with the critical domain wall width. We can basically conjecture the full domain wall width within our film structure is 9-layer thick, $1.0\times 9 = 9(\text{nm})$. The exchange energy interface between two soft layers is significant a relatively small value when $n \geq 9$. This energy corresponds to the specific switching field of maximum reduction, shown in fig.4.3.2.

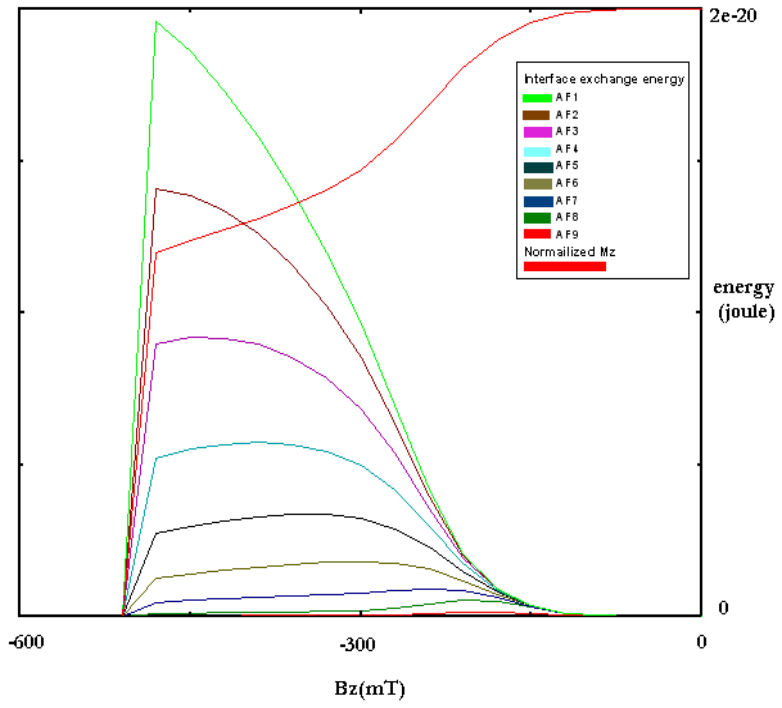

Figure 4.3.2 The curves of the interface exchange energy across each Pt spacer, and the demagnetization curve, corresponding to the varying external field.

As n is increased above a critical value, the upper soft layers encounter a much smaller energy barrier, leading to a diminished field for reversal and a small switching interval. The longer distance between the hard/soft interface and weaker coupling strength can account for this observation, due to the weaker pinning effect in the soft/hard interface domain wall propagation. In the case of hard layer, it quickly accomplishes its reversal as long as the domain breaks the interface confinement. The switching field of coupled hard layer is associated with the soft layers switching mechanism. The value decreases when n number increases, and the terminal reduced value is approximately 510 m T.

We retrieve the spin configuration of the 20 soft layers film structure in the external field of 150 m T to 510 m T. The following fig.4.3.3 demonstrates the initial saturated magnetization state at 150 m T, full-reversed state at 510 m T, as well as the transition states. This configuration can assist us to verify the domain wall propagation mechanism.

We can see the full domain wall width is 9 soft layer-thickness, forming in the pinning region of soft/hard layer interface. Another fascinating thing is that, the upper soft layers switch very fast because it can not be observed in magnetization vector data output.

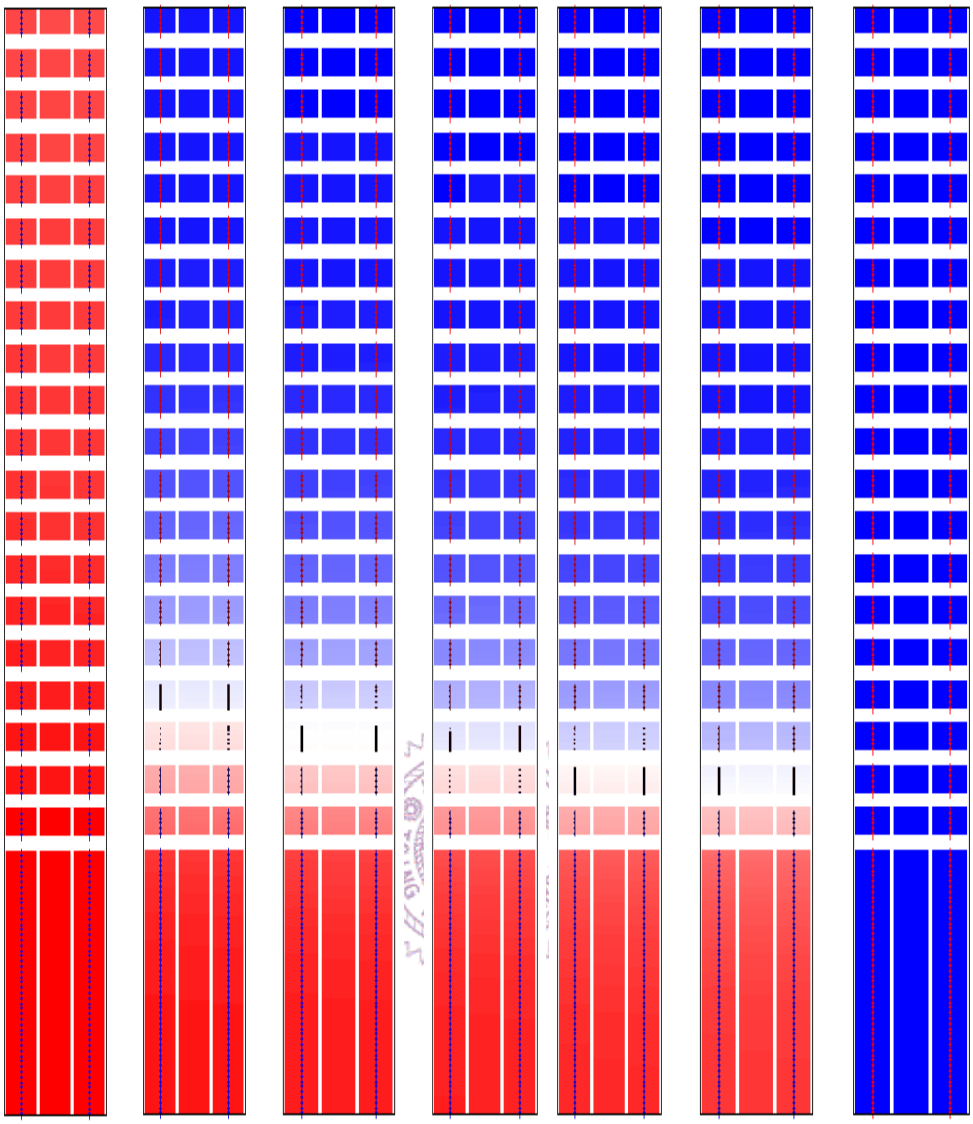

Figure 4.3.3 The domain wall transport mechanism and confining phenomenon attributed form the soft and hard layer interface in a 20 soft-layer grain structure. The external field is at 150 m T, 210 m T, 270 m T, 330 m T, 390 m T, 450 m T, 510 m T.

Instead of the full magnetization analysis, we just catch the corresponding magnetization data of top seven and the 10^{th} soft layers from the program. They almost simultaneously accomplish the reversal at a tiny region, 140 m T to 160 mT external field. As illustrated in fig 4.3.4

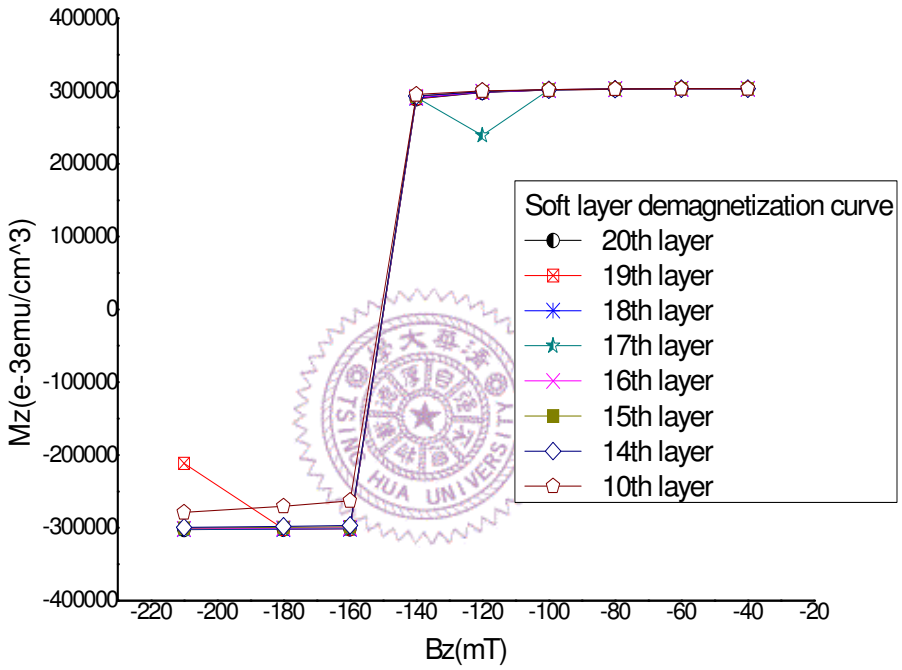

Figure 4.3.4 Time resolved demagnetization curve illustrates the upper half soft layers finish their reversal behavior in the short interval of 140 to 160 m T.

4.3.3 Conclusion

In the theory of conventional hard/soft bilayer exchange coupling system [56], the Gibbs free energy can be expressed as the following equation,

$$\varphi_t = \int_{L_s}^{0} \left\{ A_I \left(\frac{d\psi}{dz}\right)^2 + K_I \sin^2\psi - H_{ext} J_I \cos\psi + \frac{1}{2} M_I J_I \cos^2\psi \right\} dz + \int_{0}^{L_h 0} \left\{ A_\Pi \left(\frac{d\psi}{dz}\right)^2 + K_\Pi \sin^2\psi - H_{ext} J_\Pi \cos\psi + \frac{1}{2} M_\Pi J_\Pi \cos^2\psi \right\} dz$$

where A_i represents the exchange constant and K_i the first anisotropy constant. J_i denotes the spontaneous polarization, described by the angle ψ with respect to the postive easy axis, and M_i means the magnetization.

Submitted to the condition $\psi = 0$ at two layers interface and $d\psi/dt = 0$ at z is equal to L_s or L_h. The numerical solution gives the smallest nucleation field,

$$H_{N,i} = -\frac{2K_i}{J_i} + M_i - M_i \frac{l_s^2}{4L_{s,h}^2},$$

where $l_s = \sqrt{2A_I / M_I J_I}$, the exchange constant.

The first term on the right-hand side of above equation only contributes a neglect value to this nucleation field. Therefore, the ration of $\frac{l_s^2}{4L_{s,h}^2}$ dominates the magnitude of nucleation field. It is said, the negative nucleation field is achieved for $\frac{l_s^2}{4L_{s,h}^2} > 1$. This kind of

numerical model can be compared with the micromagnetic of our multilayer film structure. The energy barrier of top soft layer switching is comparatively smaller than the below one. The domain wall penetrates abruptly through the top area when the external field increases from 150 m T to 180 m T. It means the domain wall formation energy only contributes a small barrier, it can denoted as H_f , in this process. But this domain wall is finally submitted to a strong coupling force H_p , at the interface between soft and hard layer. Actually, this term dominates the critical switching field H_{sw} in a hysteresis loop. In our case, this pinning field can not be overcome until the external field exceeds 510m T.

Previous studies [57, 58] proposed the analytic solution for the depinning field of a planar domain wall in a phase interface of hard and soft layer. The field from this analytic method can be expressed as,

$$H_{dp} = \frac{2K_\Pi K_I}{J_\Pi}\frac{1-\varepsilon_k\varepsilon_A}{(1+\sqrt{\varepsilon_A\varepsilon_J})^2} - M_\Pi\frac{1-\varepsilon_k{\varepsilon_J}^2}{(1+\sqrt{\varepsilon_A\varepsilon_J})^2}$$

where $\varepsilon_A = \frac{A_I}{A_\Pi}, \varepsilon_K\frac{K_I}{K_\Pi}, \varepsilon_J = \frac{J_I}{J_\Pi}$. Comparing our numerical result with it, take $\varepsilon_A = \varepsilon_J = 1$, ε_K = 1/5 in our model. We can get the $H_{dp} = \frac{1}{5}\frac{2K_\Pi}{M_\Pi}$. This value is different from our micromagnetic result

$$H_{dp,micromagnetic} = \frac{1}{2}\frac{2K_\Pi}{M_\Pi}$$

The difference could be reasonable due to the two reasons. One is the multi-phase boundary condition in our case, another is the different

numerical method used here. One thing really remarkable is the domain wall width within this columnar grain. Because it is a control of exchange coupling in multi-soft layer film structure, the formula for estimated domain wall width, $D = 2\pi\sqrt{\frac{A}{K}}$ can be used to obtain the effective exchange constant A, by replacing the D value with the critical domain wall width observed in the micromagnetic modeling.

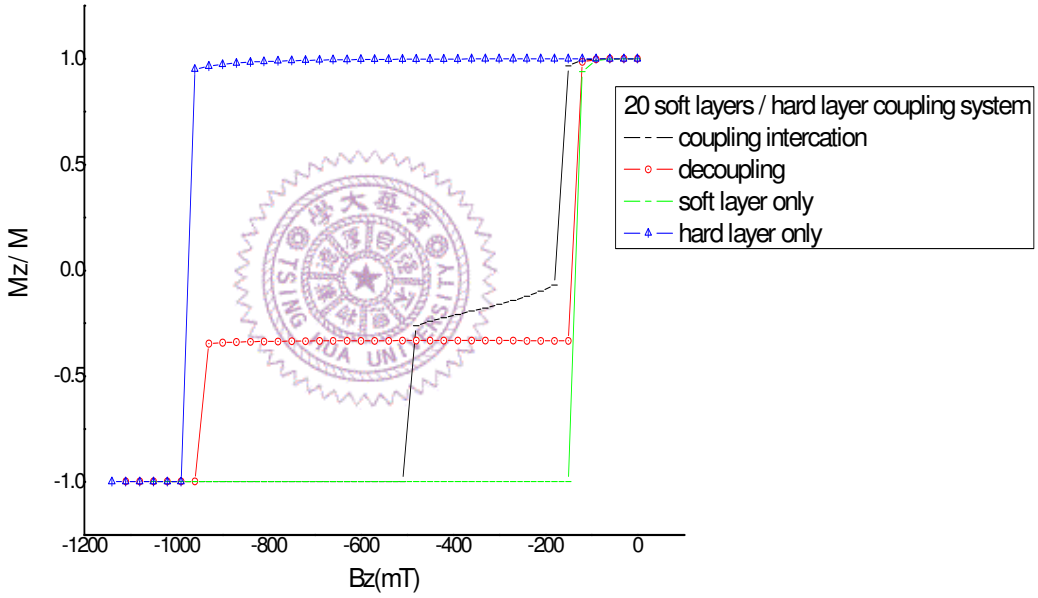

Figure 4.3.5 Demagnetization curve for 20 soft layer structure. The coupling interaction dominates the reversal behavior.

Fig.4.3.5 clearly reveals the important of the coupling interaction in our system. For the strong coupling case, a saturated field of 510 m T will be obtained. The coercivity is obviously further smaller than uniform switching case in one soft layer and one hard layer case [59].

We see the larger soft layer number boosts the soft layers reversal, which causes a reduced coercivity. To further investigate the role played by the multilayer and spacer structures, we set a model of a soft layer(9nm)/spacer(0.6)nm/hard layer(10nm) structure. It turns out that a reduced switching field can be obtained. But comparing with the case of fig. 4.3.1, N=5, the result reveals that the laminated structure enhances the coecivity-reduced effect. The reason is that, the laminated structure can induce a narrower dimension of domain wall. Comparing the spin configuration in fig.4.2.3, laminated structure and fig.4.3.6, single soft layer of 9nm thickness, the laminated structure takes more advantages due to its smaller domain wall dimension. An accompanying drawback with the thicker soft layer structure, high average M_S value in recording layer, introduces issues from the neighbor bits and DC noise. Moreover, if the increasing Ku value of the soft layer of the above soft/spacer/hard structure, the reduced switching field fails to stop increasing for a little bit. These micromagnetic simulations lead us to realize the crucial contribution of the structure in reducing switching field.

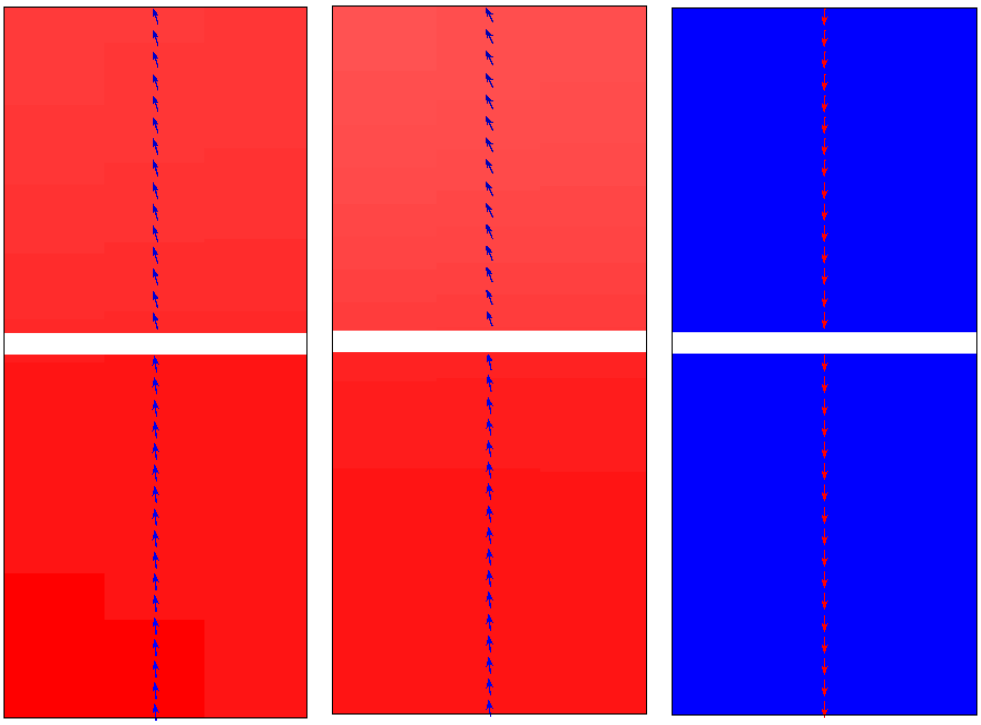

Figure 4.3.6 The vertical spin configuration inside the grain during the reversal process. From left hand side to right hand side, they are external fields of -510,-540 and -570mT. Here, soft layer thickness = 9nm, only one spacer inserted.

4.4 Double grains model

Comparing with single grain case, I want to focus on the influence of lateral coupling between soft and hard recording layers in this section. It is expected as a simplified case from cluster of a larger number grains contained.

4.4.1 Introduction

In a normal CoPtCr film structure, Cr segregation at the grain boundary

contributes to the grain isolation. This effect can be further enhanced as mentioned above by the oxygen-rich grain boundary. The optimum thermal stability is expected to be achieved when SNR is successfully diminished. Different lateral coupling strength represents the varying degree of grain isolation in this section.

4.4.2 Simulation model detail.

The grain model in this section is some rougher than the previous sections, for the purpose of being less time-consuming. Film structure and modeling parameter are as following. Soft layer number is equal to 3, soft layer thickness is 2nm, and hard layer thickness is 10nm. Spacer layer thickness is 1nm, soft/soft and soft/hard coupling strength are 0.5erg/cm^2. Other intrinsic properties are as same as the above cases. The lateral coupling strength of hard recording layer is set as zero, representing an ideal isolated granular structure. Film structure is illustrated in fig.4.4.1.

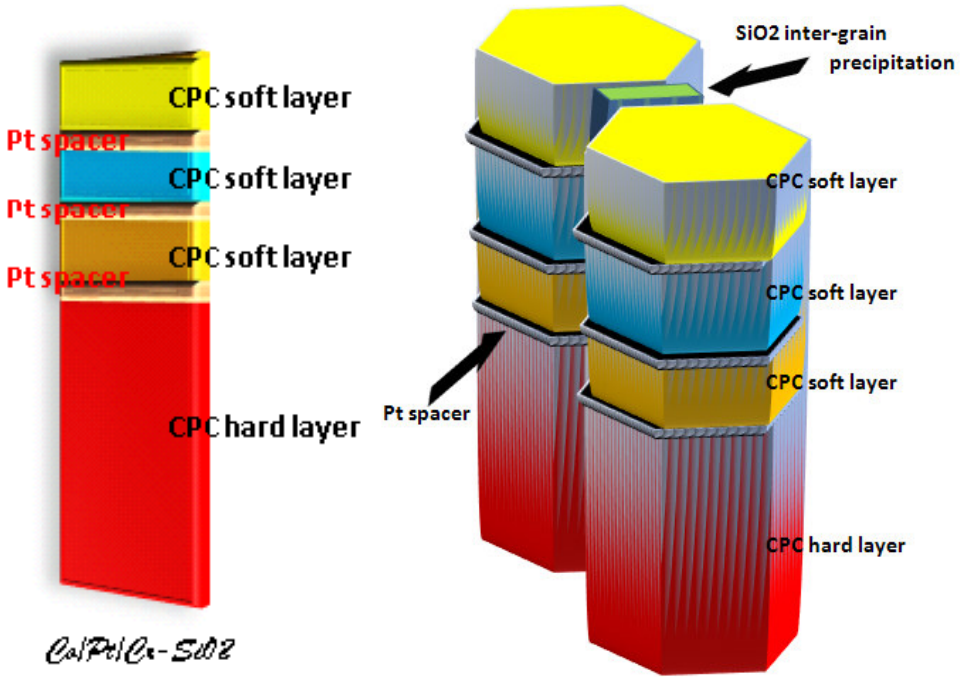

Figure 4.4.1 Extend the single grain to double grains, the upside soft layer coupling is adjusted.

4.4.3 Results and discussions

At first, it will be tested and verified if the model construction is correct in this program. The result shows that the consistency with single grain is successfully obtained. The fig.4.4.2 indicates this correspondence for different coupling strengths.

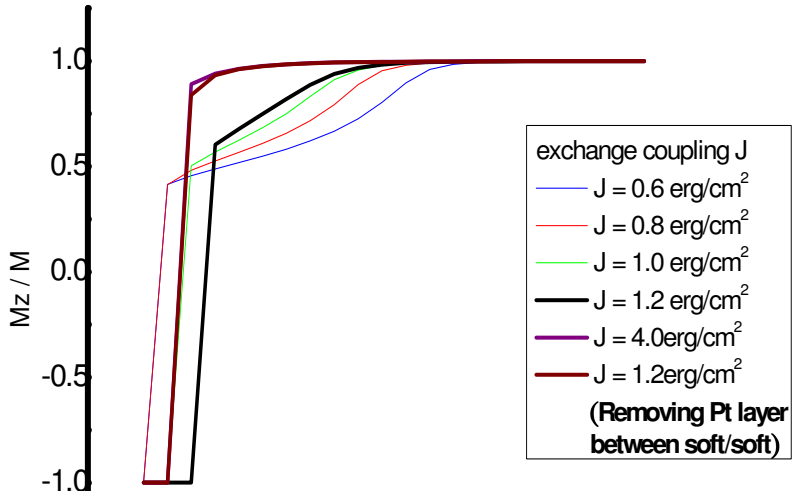

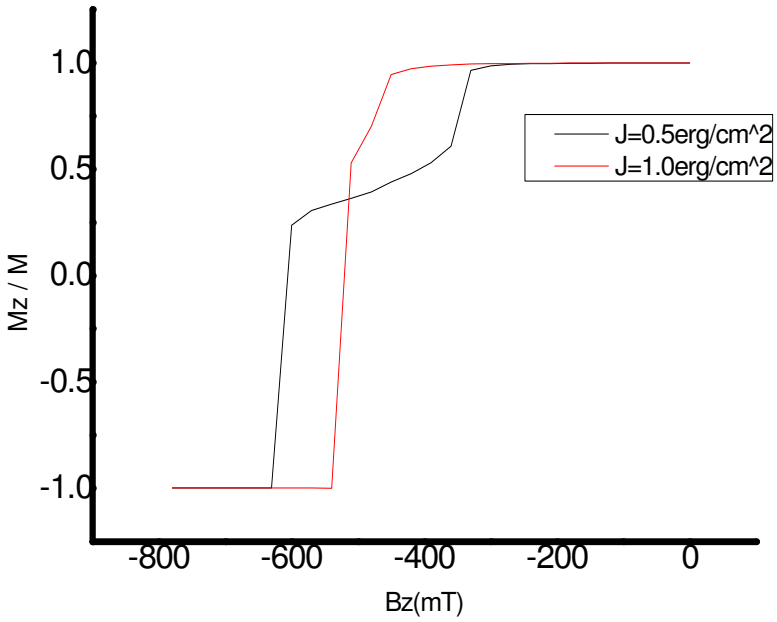

Figure 4.4.2 The corresponding demagnetization curves of single and double grains models. The top figure is single grain case, and the bottom figure is the double grain case.

An ideal isolated soft layer granular structure upside is treated as a decoupled case. Enhancing the coupling intensity to 2.56 erg/cm^2, an increasing nucleation field and saturation field gradually appear. Simulation results are presented in fig.4.4.3.

The purpose of experiment in this section is to investigate the mechanism between the conventional granular ECC structure and the continuous granular coupled (CGC) media structure. When the lateral grain coupling effect is enhanced, the saturation field and nucleation field consequently increase. This phenomenon can be seen as soft/soft layer lateral coupling strength $J_U > 1.28\, erg/cm^2$. But actually, we can not

get batter magnetization property in the condition of strong J_U from our simulation result.

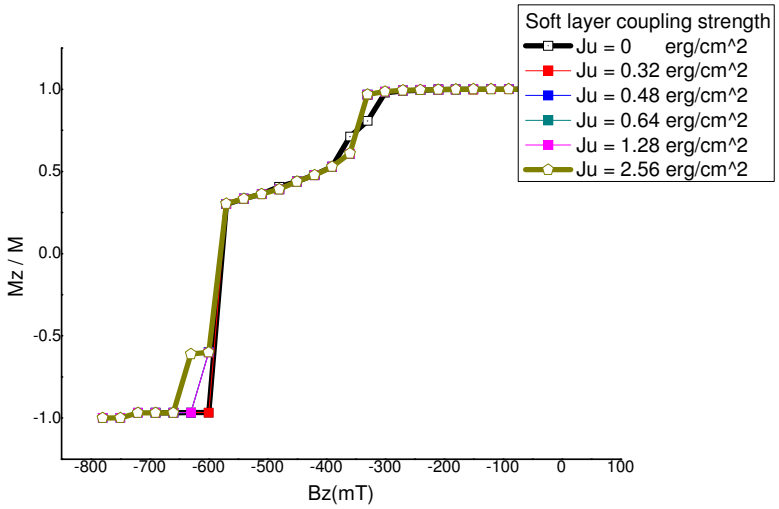

Figure 4.4.3 The demagnetization curve of different degree of the grain isolation.

4.4.4 Conclusions

The basic concept of CGC media [60, 61] is to combine a continuous layer and a granular recording layer by strong direct exchange coupling. The continuous layer contributes to the large thermal stability and the granular structure provides high resolution. In this section, we eventually fail to reach the benefit of stronger J_U. This result may has something to do with the following two reasons. First, each grain sustains an in-plane anisotropy exchange coupling force. It induces an anomalous spin configuration within each grain. Second, the coupling strength between soft and hard layer is not strong enough to support the reversal mechanism of hard layer. It should be noticed that, the coupling strength between continuous and granular layer is very strong in the initial CGC

media concept.

4.5 Seven-grain cluster model

To be more approximate the real case, the lateral exchange coupling interaction linking up every neighboring grain can not be neglected any more. The strategy here is to take a 7-grain cluster reciprocal coupling force into consideration, then only pick up the center grain information. This implementation is indeed more time- consuming than other previous models.

4.5.1 Introduction

This cluster is regarded as the smallest unit in a periodic boundary condition case. Of course, only the first circle of neighboring grains directly touching the center grain contribute coupling to this system. Finally, when picking up simulation result, a rectangle region most approaching the hexagonal basal is retrieved by special code controlling. It is a feasible method to obtain the tendency in multi-grains coupling system.

4.5.2 Simulation model detail.

As same as the extension from single grain to double grains, the intrinsic properties remain. But due to the complication of a large amount of the lateral and longitudinal coupling forces, inside and outside the grains, different film structures are constructed. My program algorithm is to define the geometry by code script and image file, then establishing the

vector filed in this simulation domain. So I can set the coupling force according to specific vector direction and distance. Here different meshes sizes are used, because the value is sensitive for the algorithm to catch the precise interface between each region. The top view of defined structure is demonstrated in fig.4.5.1.

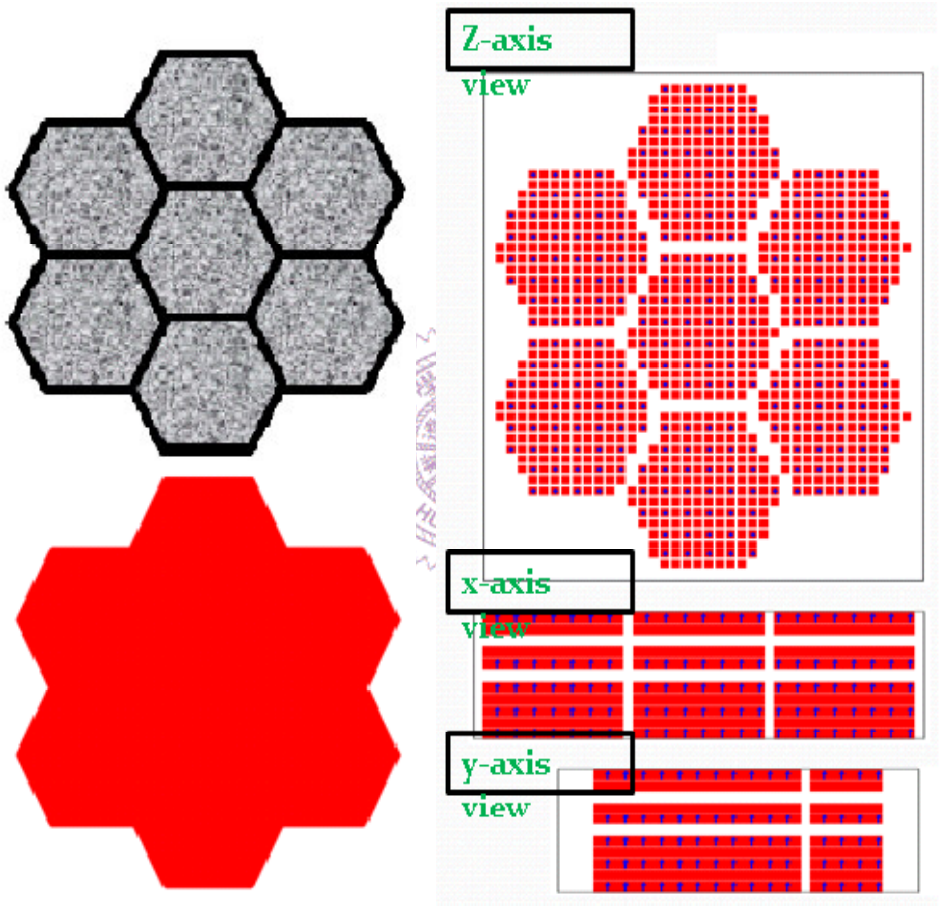

Figure 4.5.1 The up left-hand side is the granular structure, and bottom left-hand side is the continuous film structure. The right-hand side is the top and cross section view in mesh and initially saturated spin configuration.

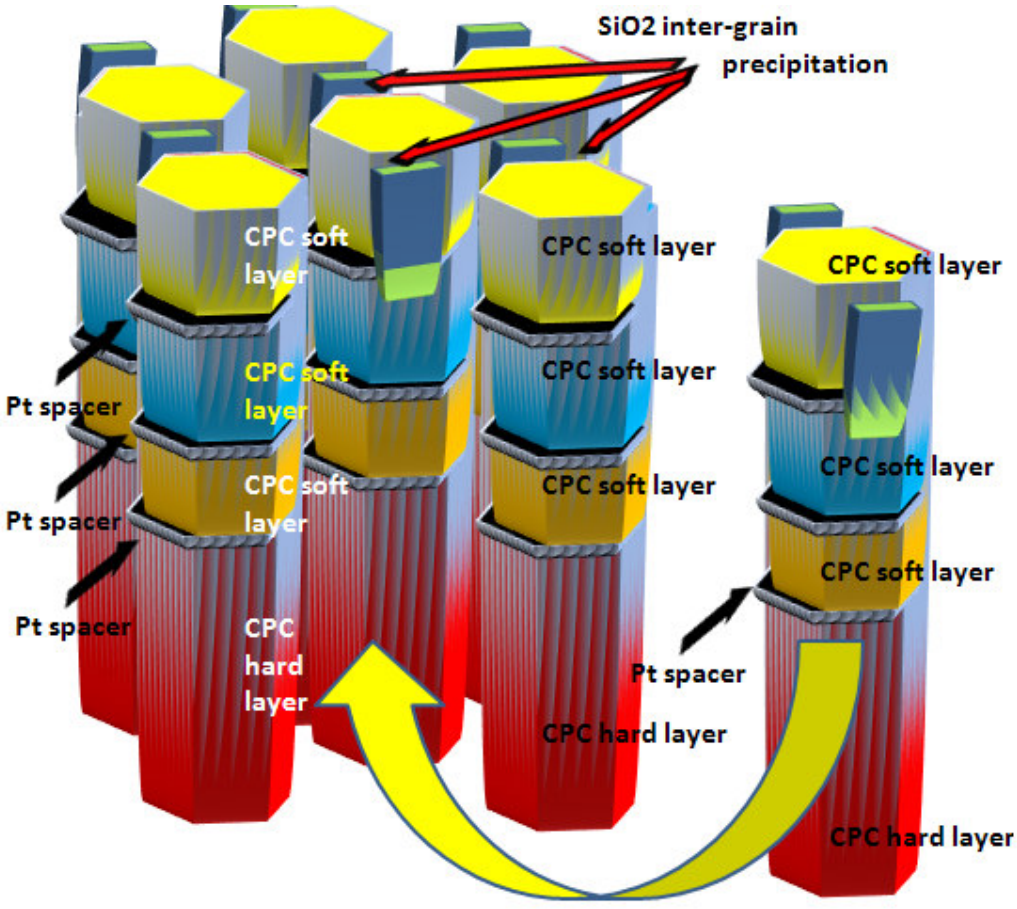

Figure 4.5.2 The illustration of 7-grain cluster model.

4.5.3 Results and discussions

The next fig.4.5.3 is a model of two-soft layer over one-hard layer structure. The film thickness for soft layer, spacer, and hard layer are 2nm, 1nm, and 5nm, respectively. The intrinsic properties parameters are as above section. And the coupling strengths inside and between the grains are 0.5erg/cm^{2}and 0.32 erg/cm^2, respectively. An experimental result is also present in fig.4.5.4 for comparison.

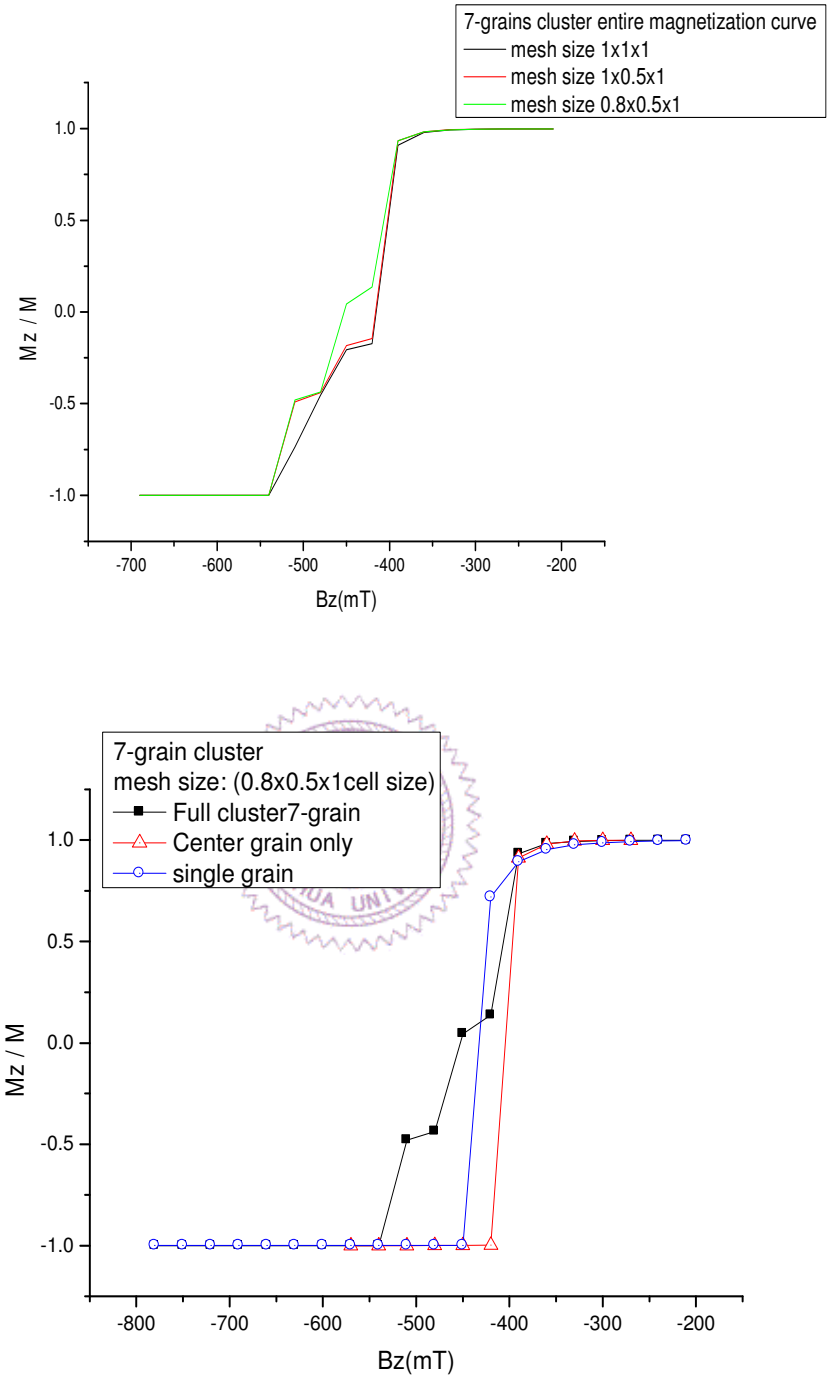

Figure 4.5.3 The demagnetization curve with different mesh sizes (upside figure). The bottom figure reveals the center grain in cluster model can further reduce the switching field.

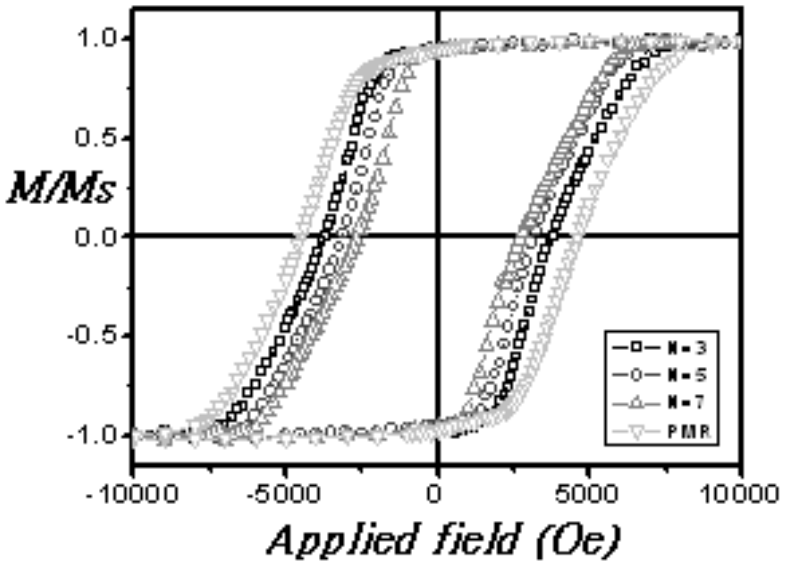

Figure 4.5.4 The measured MH loop for different soft layer number. Experiment is conducted by Hao-Cheng Hou.

In the first curve of fig.4.5.3, it is known the cell size will be a critical fact in this model. Refined mesh precisely defines the basal plane of each grain and the corresponding coupling force. If the mesh construction is not delicate enough, the demagnetization curve will approach a single grain dominating behavior.

It is remarkable that, comparing with single grain analysis in section 4.2, the impact of lateral coupling force can not be neglected in this system. The soft layer number and inside-grain layer coupling force are reduced relative to the condition in section 4.2(fig.4.3.1with n=3, inside-grain layer coupling J=1.2 erg/c m^2). The H_C and H_S are expected to increase to a value about 650 m T according to the discussion

in section 4.2. But it turns out that the H_C decays to 450 and 410 m T for full cluster and center grain, respectively. Return to the condition hypothesis posed at the beginning of this study, we can claim this modeling is accurate.

The following fig.4.5.5 and fig.4.5.6 are more complicated 7-grain cluster models. In principle, the Hc increases when the dimension of model increases (this can be due to the larger Mtotal). So the simulation shows a larger Hc in N=3, comparing with N=2. But if soft layer number keeps increasing, being able to contain more parts of domain wall, the Hc is finally reduced. It is shown in previous single grain case.

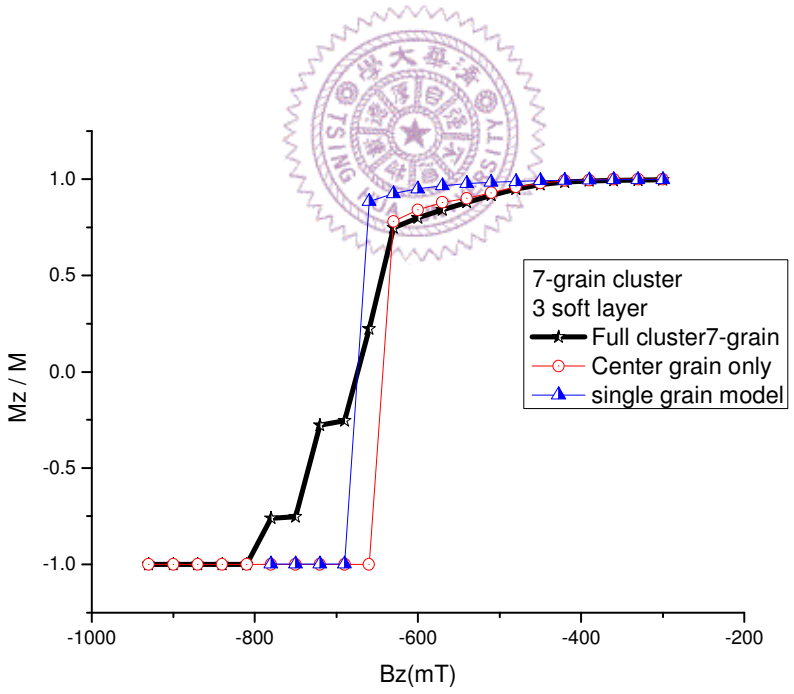

Figure 4.5.5 The demagnetization curve of more complicated 7-grain cluster model(3 soft + 1 hard within each grain).

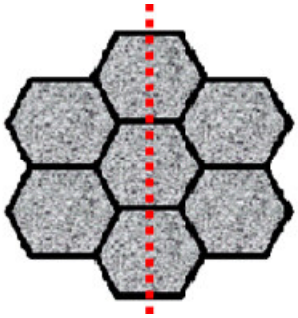

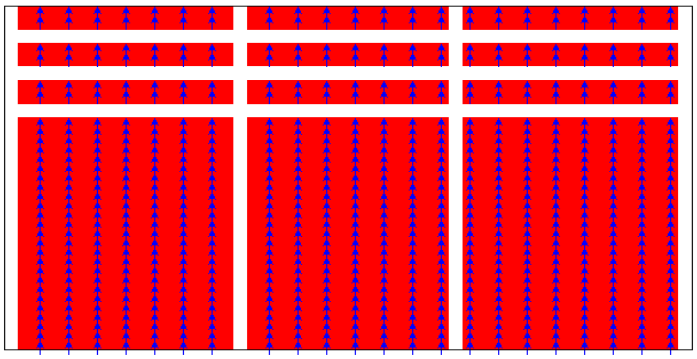

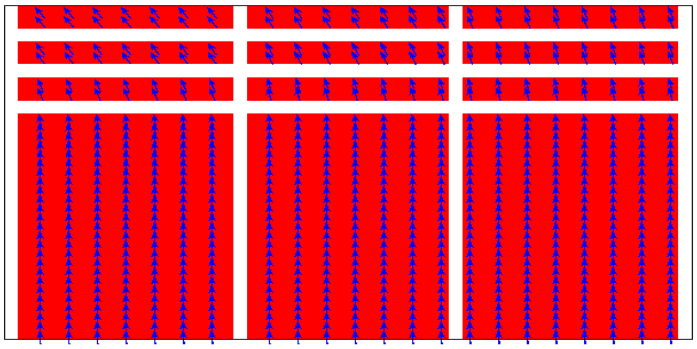

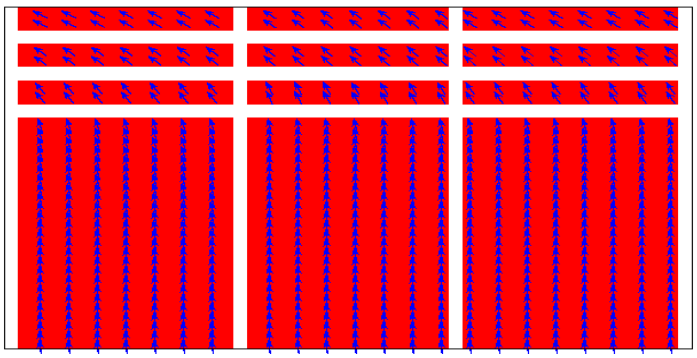

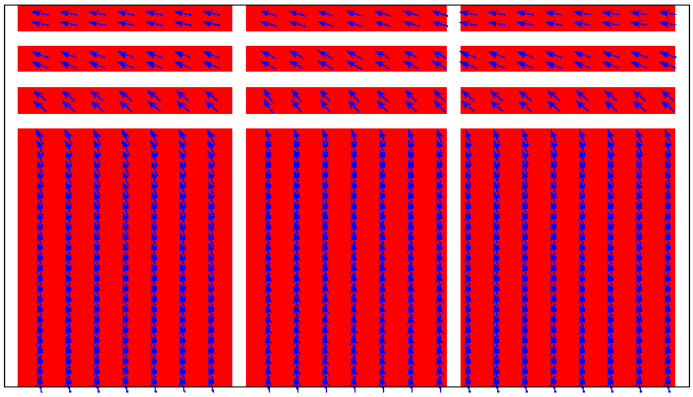

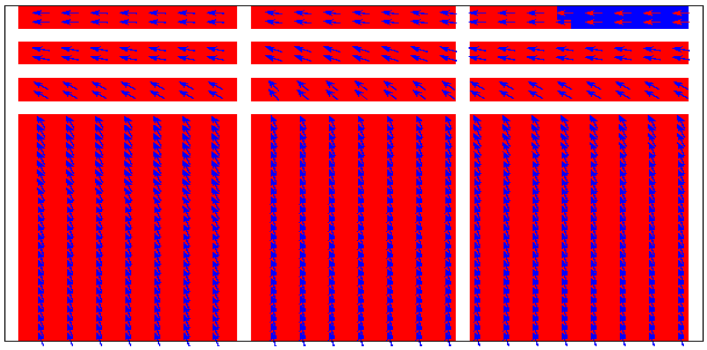

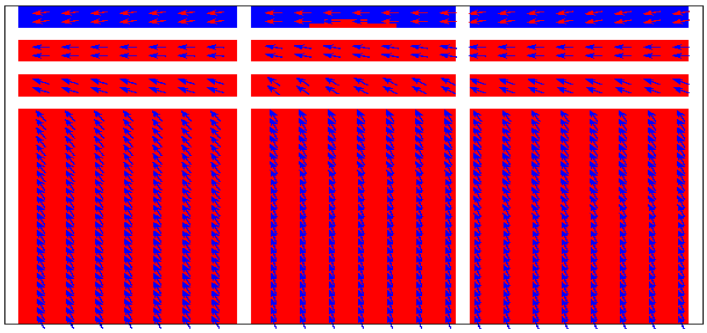

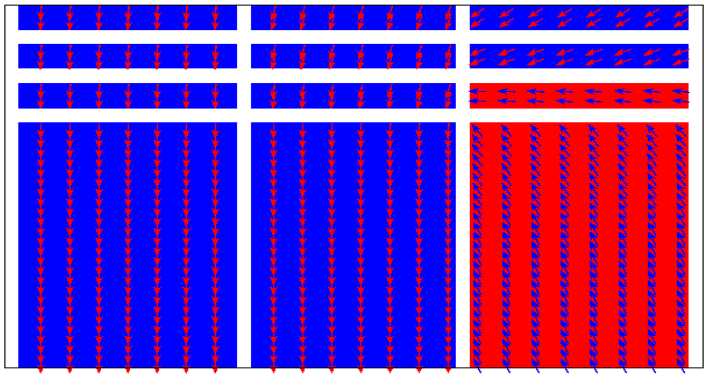

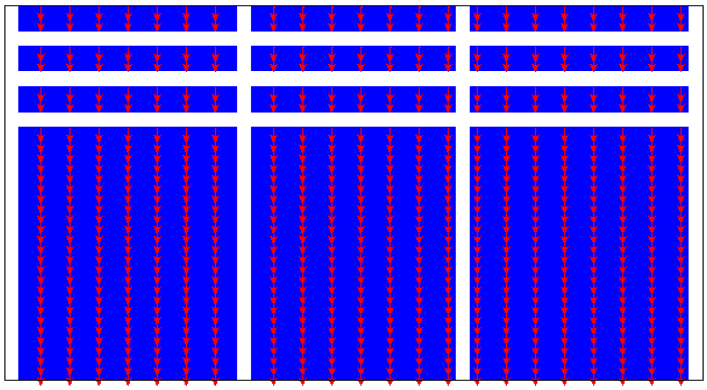

Figure 4.5.6 The spin configuration of more complicated 7-grain cluster model(3 soft + 1 hard within each grain), positive z-axis saturation to negative z-axis saturation . The in-plane magnetic reversal is obviously non-coherent.

Because the lateral coupling forces are set between the soft assisting layers and the hard recording layers, so it is not an ideal isolated granular film structure. This lateral interaction acts as a chain to restrict the magnetization in each grain. In the case of structure with 2 soft layers, the center grain reverses at a relatively small field of 410 m T, and the loop shape of whole cluster further approaches the experiment data. It can be seen in fig.4.5.3 and fig.4.5.4. The fig. 4.5.6 illustrates the dynamic magnetization in this cluster. We can observe that it is the mechanism like so-called L-shaped vortex in this small size model. In this vortex switching model, the effective torques in each parts of each grains are not equal. This phenomenon leads to an obviously asymmetric switching in each grain. The reversal of center grain is partially induced by the lateral coupling strength from the neighboring grain which has finished its

reversal. And this center grain also exerts a coupling force to reverse the nearby grain un-reversed.

However, the 7-grain cluster is still a small region modeling, so the edge side is highly possible to be subjected to the shape anisotropy. Of course, the in-plane magnetization random distribution dose not significantly affect the out-of-plane magnetization.

4.5.4 Conclusions

In principle, micromagnetic simulation has some deviations from real cases. So we can rationally predict the effects of rectangle-approached grain boundaries, which are not precisely hexagonal. In my programming, the inter-grain coupling forces may fail to be accurately defined in the boundaries. However, these deviations are still tolerable in the numerical process. Here we can arrive at the conclusion by the discussions above. That is, the reduction of H_C of the center grain in the grain-cluster model introduces the lateral coupling interactions. This case can further approach our experimental result. It makes sense because the center grain is set in the more realistic soundings.

Chapter5 Summary

1. The Pt spacer acts as a pinning site confining the magnetization distribution in this multilayer structure. Controlling its strength by modifying the Pt layer thickness, we can change the interface energy barrier between soft layers.

2. Increasing coupling interaction from $J = 0.6 erg/c\ m^2$ to $J = 1.2 erg/c\ m^2$ can reduce the energy barrier of magnetization penetrating the spacer. But there is an optimum J value leading to a most reduced coercivity.

3. Enhancing the soft layer number promotes the domain wall assisting reversal in our film structure design. This mechanism can successfully reduce the domain pinning effect, corresponding to a smaller coercivity. Moreover, the importance of laminated structure really emerges from the above single grain modeling. It is due to the smaller domain wall width in the multilayer comparing with the single layer structure. This kind of special structure design obviously improves the magnetic property.

4. The center grain of the 7-grain cluster shows a reduced coercivity, which more approaches our experiment data. It can be contributed form the lateral coupling effect and demagnetization field.

5. Even the double or the 7-grain cluster are relatively local regions, the periodic boundary condition should be used to improve the reality of this modeling. Certainly, the time-consuming issue is always a key issue here.

Reference

[1] Zhihong Lu P. B. Visscher, and Butler, IEEE Vol. 43, No. 6.

[2] D. Goll, S. Macke, H. N. Bertram, APL 90, 172506.

[3] L. D. Landau, E. M. Lifshitz, Phys. Z. Sowietunion 8, 153(1935).

[4] W. F. Brown Jr, Micromagnetics, Interscience Publishers(1963).

[5] T. L. Gilbert, Physical Review, 100(1955), p. 1243.

[6] Chantrell, R. W., Hannay, J. D., Wongsam, M., Schrefl, T., and Richter, H.-J., 1998, IEEE Trans. Magn. 34, 1839.

[7] Chantrell, R. W., Hannay, J. D., Wongsam, M., Walmsley, N and Schrefl, T., 1997, J.Magn. Magn. Mater. 175, 137.

[8] Chantrell, R. W., 1997, 'Interaction Effects in Fine Particle System'. In Magnetic Hyteresis in Novel Magnetic materials (Ed. G.C. Hadjipanayis, Kluwer Academic Publ. Dordrecht)p. 21.

[9] Tako, K.M., Wongsam, M., and Chantrell, R.W., 1996, J. Appl. Phys. 79, 5756

[10] Schmidts, H.F., and Kronmuller, H., 1991, J.Magn. Magn. Mater. 94,220

[11] Brown, W. F., 1940 Phys. Rev. 58. 736.

[12] Brown, W. F., 1941 Phys. Rev. 60. 132

[13] Kittel, C., and Galt, J.K., 1956, Solid State Phys. 3, 437

[14] Brown, W. F., Jr., 1963 Micromagnetics

[15] Aharoni, A., 1996, Introduction to the Theory of Ferromagnetism

[16] Chikazumi, S., 1997, Physics of Ferromagnetism

[17] Jiles, D., 1990, I ntroduction to Magnetism and Magnetic Materials

[18] P. Weiss, L'Hypothese du champ Moleculaire et de la Propriete Ferromagnetique, J. de Phys. 6, (1907)

[19] H Neal Bertran, and Jian-Gang Zhu, Solid State Physics, vol.64, 1992

[20] Brown, W. F., Jr., Micromagnetics, Interscience Publishers, 1963

[21] A. Aharoni, Introduction to the Theory of Ferromagnetism, Oxford University Press(2001)

[22] M. d'Aquino, C. Serpico, and G. Miano I. D. Mayergoyz G. Bertotti, J. Appl. Phys. 97, 2005

[23] D. Suess, V. Tsiantos, T. Schrefl, W. Scholz, and J. Fidler, J. Appl. Phys. vol. 90, 2002

[24] Josef Fidler and Thmas Schrefl , J. Phys. D: Appl. Phys. 33(2000)

[25] F. Garcia-Sanchez, O. Chubykalo-Fesenko, O. Mryasov, R. W. Chantrell, JMMM 0 (2005)

[26] F. Garcia-Sanchez, O. Chubykalo-Fesenko, O. Mryasov K. Yu. Guslienko, R. W. Chantrell, Appl. Phys. Lett. 87(2005)

[27] H. Kronmuller, R. Fischer, R. Hertel, T. Leineweber, J. Magn. Magn. Mater. 177(1997) 175.

[28] H. Kronmuller, M. Bachmann, Physica 96(2001) B306.

[29] R. H. Victora, X. Shen, IEEE Trans. Magn. 41(2005) 537

[30] I. Takekuma, R. Araki, M. Igarashi, H. Nemoto, I. Tamai, Y. Hirayama, and Y. Hosoe, J. Appl. Phys. 99, 08E713 (2006)

[31] P. Skomski, J.M.D. Coey, Phys. Rev. B 48 (1993) 15812.

[32]D. Suess, T. Schrefl, S. Fahler, M. Kirschner, G. Hrkac, F, Dorfbauer, J.Fidler, Appl. Phys. Lett. 87(2005)012504

[33] T. Schrefl, J. Fidler, H. Kronmuller, Phys. Rev. B 49 (1994) 6100.

[34] H. Kronmuller, D. Goll. Phys. B: Condens. Matter 319 (2002) 122.

[35] P.N. Loxley, R.L. Stamps, IEEE Trans. Magn. 37 (2001) 2098.

[36] MJ. Donahue, D.G. Porter, OOMMF User's Guide, Version 1.2 ahpa 3, NIST, Gaithersburg MD, 2002

[37] H. Kronmüller, D. Goll's work[Physical B 319(2002) 122-126]

[38] A. Yu. Dobin and H. J. Richter, APL 89, 062512(2006)

[39] Dieter Suess, J. Magn. Magn. Mater. 308, 2007

[40] H. Kronmüller, and Manfred Fähnle, Micromagnetism and the Microstructure of Ferromagnetic Solid, Cambrige University Press, 2003.

[41] Dieter Suess, Thomas Schrefl, Josef Fidler, IEEE Trans. Magn. Vol. 37, No. 4, July 2001

[42] Massimiliano d'Aquino, Nonlinear magnetization dynamics in thin-films and nanoparticles, 2004

[43] K. Z. Gao and N. Bertram, IEEE Trans. Magn. 38, 3675(2002)

[44] T. Leineweiber, H. Kronmüller, Phys. Stat. Sol. (b) 201 (1997) 291.

[45] A. Yu. Dobin and H. J. Richter, Appl. Phys. Lett. 89, 062512(2006)

[46] A. Goncharov, T. Schrell, G. Hrkac, J. Dean, and S. Bance , D.

Suess, O Ertl, F. Dorfbauer, and J. Fidler , Appl. Phys. Lett. 91 222502(2007)

[47] Amikam Aharoni, J. Appl. Phys. vol. 83, 1998

[48] Michael J. Donahue, Donald G. Porter, Physica B, 343 (2004) 177-183

[49] Michael J. Donahue, R.D. McMicheal, IEEE Trans. Magn. Vol. 33, 4167-4169(1997)

[50] Michael J. Donahue, Donald G. Porter, OOMMF Programming Manual, release 1.2a3, November 18, 2005

[51] H. Muraoka, Y. Sonobe, K. Miura, A. M. Goodman, and Y. Nakamura, IEEE Trans. Magn. Vol. 38, No. 4, July 2002

[52] P. F. Carcia, J. Appl. Phys. vol. 63, p.5066, 1998

[53] R. M. Bozorth, P. A. Wolff, D. D. Davis, V. B. Compton, and J. H. Wernick, Phys. Rev. 122, 1157(1961).

[54] K. V. O'Donovan, et al., Phys. Rev. Lett. 88(2002) 067201

[55] Kai-Zhong Gao, Juan Fernandez-de-Castro, and H. Neal Bertram2, Fellow, IEEE Trans. Magn. Vol. 41, No. 11, Nov 2005

[56] D. Goll, H. Kronmüller, Physica B, 403 (2008) 1854-1859

[57] H. Kronmüller, H.-R. Hilzinger, J. Magn. Magn. Mater. 2 (1976) 3.

[58] D. Goll, H. Kronmüller, Physica B, 319 (2002) 122.

[59] Jian-Ping Wang, Weikang Shen, Jianmin Bai, IEEE Trans. Magn. Vol. 41, No. 10, July 2001

[60] H. Muraoka, Y. Sonobe, K. Miura,A. M. Goodman, and Y. Nakamura, IEEE Trans. Magn. Vol. 38, No. 4, Sep 2002

[61]Y. Sonobe, H. Muraoka, K. Miura, Nakamura, K. Takano, A. Moser, H. Do, B. K. Yen, Y. Ikeda, N. Supper, and W. Weresin, IEEE Trans. Magn. Vol. 38, No. 5, Sep 2002

[62] Hans Fangohr and Thomas Fischbacher at the University of Southampton, http:// nmag.soton.ac.uk /nmag/index.html)